2018

GEOCHEMISTRY OF HIGHLY ALKALINE WATERS OF THE COAST RANGE OPHIOLITE IN CALIFORNIA, USA

Mahrukh Shaikh
University of Rhode Island, mahrukh79@gmail.com

GEOCHEMISTRY OF HIGHLY ALKALINE WATERS OF THE COAST RANGE OPHIOLITE IN CALIFORNIA, USA

BY

MAHRUKH ANWAR

A THESIS SUBMITTED IN PARTIAL FULFILLMENT OF THE REQUIREMENTS FOR THE DEGREE OF

MASTER OF SCIENCE

IN

BIOLOGICAL AND ENVIRONMENTAL SCIENCES

UNIVERSITY OF RHODE ISLAND

2018

MASTER OF SCIENCE IN BIOLOGICAL AND ENVIRONMENTAL SCIENCES

OF

MAHRUKH ANWAR

APPROVED:

Thesis Committee:

Major Professor Dawn Cardace

Ali Akanda

Soni Pradhanang

Nasser H. Zawia
DEAN OF THE GRADUATE SCHOOL

UNIVERSITY OF RHODE ISLAND
2018

ABSTRACT

Altered waters impacted by serpentinization of Coast Range Ophiolite (CRO) ultramafic units have been reacting with trapped Cretaceous seawaters, meteoric waters, and other surface derived waters since tectonic emplacement of this ophiolite. In 2011, groundwater monitoring wells of various depths were established near Lower Lake, CA, USA in the McLaughlin Natural Reserve, administered by the University of California-Davis, in order to understand ongoing low temperature alterations and biogeochemical interactions taking place. Wells were installed at two sites in the Reserve. There are three Quarry Valley area wells (QV1-1 [23m depth], QV1-2 [14.9m], QV1-3 [34.6m]) and five Core Shed area wells (CSW1-1 [19.5m], CSW1-2 [19.2m], CSW1-3 [23.2m], CSW1-4 [8.8m], CSW1-5 [27.4m]). Water samples were collected from all installed wells, as well as from an older well drilled near the historic core shed (Old Core Shed Well, or OCSW [82m]), and an upper (TC1) and lower (TC2) site sampling a nearby groundwater-fed alkaline seep, at Temptation Creek. Key environmental parameters (temperature, pH, conductivity, oxidation-reduction potential, and dissolved oxygen) were collected in the field using YSI-556 multiprobe meter, and total concentrations for major cations (Ca^{+2}, Na^{+}, Mg^{+2}, K^{+}) were analyzed using Thermo Scientific iCAP 7400 Inductively Coupled Plasma-Atomic Emission Spectrometry, and anions (F^{-}, Cl^{-}, SO_4^{-2}, NO_3^{-}) on Dionex Modular DX 500 Ion Chromatography.

Principal component analysis was conducted to determine key factors and processes controlling water chemistries at CRO. Geochemist's Workbench software was used to model the low temperature alteration of a serpentinization-influenced

model water volume passing through serpentinite over a period of 100 million years. Modeling provided insight into the changing pH, Eh, evolving water chemistries, stepwise mineral assemblages, appearance of marker minerals at geochemical transitions in the system, and supported evidence of pervasive impacts of low temperature, oxidative weathering of serpentinites. This work supports the case of incremental dilution and transformation of a deeply sourced Ca^{2+}-OH^{-} Type II water in this environment, and constrains reaction status of present day CRO waters and those of similar sites, in terms of the progress of serpentinite weathering reactions. Further, the study informs our understanding of serpentinization-related geological environments present on other celestial bodies (*e.g.*, Mars, Europa, Enceladus) in our Solar System and beyond.

ACKNOWLEDGMENTS

It is not very often that we come across people who go above and beyond to help, reach out and support in every way possible. For me, it has been Dr. Dawn Cardace. She was my mentor the day I started my undergraduate studies at the Department of Geosciences, at the University of Rhode Island. I had no idea then that I would have the good fortune of returning back for a master's program under Dr. Cardace caring mentorship. She has been my guiding light, my anchor, and my rock for all these years at URI. I can never thank her enough for all that she did for me.

I would also like to thank my thesis committee, Dr. Ali Akanda and Dr. Soni Pradhanang, and my defense chair Dr. Alison Tovar, and my Geology Department professors: Dr. Boving, Dr. Engelhart, Dr. Fastovsky, Dr. Laliberte, Dr. Pradhanang, Dr. Savage, and Dr. Veeger. A special thank you to Julie Smallridge, and Ken Wilkinson. I would also like to thank all my departmental colleagues, especially Khurshid, Michaela, Reilly, and Jordanne.

Alex, Marzia, Jeeban: thank you for being wonderful officemates. I enjoyed every minute I got to spend with you all in our tiny yet welcoming office.

Roger: thank you for always checking on how I am doing, for always encouraging, and for the big smiles and hugs, and last but not least, our mutual love of anything automobile-related.

Alex: I have lost count of the number of times you ran to print pages for me on a minute's notice for our meetings. Thank you for everything you have done, including helping with the move and for sharing Trevor Noah You-Tube clips.

Meg: you were like a sister for me from the first day we met. From stickers, museum tickets, delicious home cooked meals, you were always there to hug me and tell me "Mahrukh, it will be okay!" And it was.

Alex, Meg, Roger: I will miss all the times we spent together gathered around the big table for our meetings with Dr. Cardace.

I would like to acknowledge and thank my loving and supportive family for not letting me give-up, for supporting me through all these years, and for being there for me through thick and thin. Mom and dad, my siblings Naushin, Khurram, and Sania, brothers in laws Naeem and Nabeel, and my nephew and niece Ayman, and Asra. Thank you all so much!

To my daughters, Aiza and Rania: I love you both more than words can describe. Thank you for understanding all the times you both endured my submission deadlines and finals, for never complaining about me not being able to spend more family time and weekends out of the house. Rania, thank you for accompanying me to my college all these years and attending the classes with me since you were five years old. Aiza, I cannot forget all the times you spent in the lab with me patiently waiting for me to finish my work so we could go home.

I would also like to recognize the support and funding from the University of Rhode Island, College of Environmental and Life Sciences for teaching assistantship, NASA Astrobiology Institute CAN7 Rock Powered Life Award to Co-Investigator Cardace (Solicitation # NNH13ZDA017C), and NASA Rhode Island Space Grant College and Fellowship Program, Space Grant Opportunities in NASA STEM

(Solicitation #NNX15AI06H). I would also like to thank Joseph Orchardo for helping with the use of equipment necessary for this research at Brown University.

PREFACE

This document is prepared in manuscript format and adheres to the style of the scientific journal *Chemical Geology.*

TABLE OF CONTENTS

LIST OF TABLES

LIST OF FIGURES

MANUSCRIPT

This manuscript is prepared for submission to the *Chemical Geology*.

INTRODUCTION

The Coast Range Ophiolite (CRO) is a tectonized mélange of units of the oceanic lithosphere, stretching north of San Francisco area in California, U.S.A. (Cardace et al., 2013). Here, the Middle to Late Jurassic CRO exposures represent deformed and structurally dismembered segments of oceanic crust and uppermost mantle, now incorporated within the continental block (Dickinson et al., 1996), that are undergoing a unique process of long-term aqueous alteration, characterized as vigorous serpentinization (Figure 1) followed by low temperature, oxidative weathering.

Serpentinization is the process during which ultramafic mantle rocks rich in olivine and pyroxene react with water, leading to formation of serpentinite rock that is dominated by serpentine group minerals including lizardite, chrysotile and antigorite (Moody, 1976). This water-rock reaction is accompanied by the generation of fluids with high concentrations of hydrogen (Corliss et al. 1981; Russell, 2007; Ehlmann et al, 2010), increase in rock volume, and release of heat energy (Allen and Seyfried, 2004). Serpentinization can be summarized as:

olivine + water → serpentine + brucite + magnetite

$$(Mg,Fe)_2SiO_4 + H_2O \rightarrow (Mg,Fe)_3Si_2O_5(OH)_4 + (Mg,Fe)(OH)_2 + Fe_3O_4 + H_2$$

$$2(FeO)_{rock} + H_2O \rightarrow (Fe_2O_3)_{rock} + H_2$$

Here, the parent mineral olivine, containing magnesium, iron, silicon, and oxygen, reacts with H_2O resulting in the oxidation of iron from ferrous ions (Fe^{+2}) to ferric ions (Fe^{+3}), while the water molecules are reduced to hydrogen gas and

hydroxide ions (OH^-). These OH^- ions drive the pH of the serpentinizing waters to high alkaline levels. Coast Range Ophiolite is one of the rare, well documented sites where these hyperalkaline waters exist (Figure 2).

The process of serpentinization has recently gained attention due to the production of highly reducing environments enriched in molecular hydrogen and methane, all of which can provide microbial communities with chemical energy that can sustain biomass--providing favorable living conditions within the deep biosphere. Life support by chemical energy instead of photosynthesis has provided prospects for life's existence on other celestial bodies like Mars and Jupiter's moon Europa (McCollom et al., 2013). The characteristic mineralogy and aqueous geochemistry at Earth-based serpentinizing sites are analogous to subsurface Martian environments, where the altered olivine-rich rocks (olivine detections, Koeppen et al. 2008, serpentine detections, Ehlmann et al., 2010) suggest occurrence of serpentinization in past. In fact, serpentinization may be ongoing in the subsurface, with some evidence for continuing groundwater flow (Michalski et al., 2013), conveniently sheltered from sterilization by incoming cosmic radiation on the surface of Mars (Zeitlin et al., 2004). Simultaneously, this ability of microorganisms to survive also provides explanation and insight into synthesis of organic compounds needed in the origination of life on Earth (Lang et al., 2010, Martin et al., 2008).

Another important area of significance and ongoing research involves serpentinization for its role in carbon sequestration (carbon capture and storage, CCS). The hyperalkaline serpentinizing waters contain almost no dissolved inorganic carbon (DIC). When these waters reach the surface or get discharged, atmospheric carbon

dioxide is rapidly taken up and converted into insoluble carbonates (Burns & Matter, 1995; Chizmeshya et al., 2007; Andreani et al., 2009; Kelemen et al., 2011; Paukert et al., 2012). This presents a way to store the increasing and alarming concentrations of carbon dioxide from the atmosphere and is now an active area of ongoing research with a promising potential of reversing the effects of anthropogenic global warming (McCollom et al., 2013).

Given these recent scientific research interest in serpentinites, the objective of this paper is to develop a more thorough understanding of the serpentinite weathering, geochemistry of the serpentinizing fluids, serpentinite rock-water interactions, and changes in mineralogy and fluids chemistry with the passage of time.

The interaction of the serpentines with water and causing the resulting waters to undergo unique chemical changes was first reported and studied by Barnes and colleagues in 1967. Barnes compared the ionic concentrations of the unusual ultrabasic spring samples from Red Mountain in California, John Day in Oregon, and Cazadero in California, and proposed that these unusual waters were genetically related to serpentinization (Barnes et al., 1967). Later, in 1977, Barnes and O'Neil compared the pH, ionic makeup, and other compositional properties of the water samples collected from the serpentinizing sites in New Caledonia and Yugoslavia and compared those with the samples from Oman (collected by Bailey and Coleman), and the samples from Oregon and California. Barnes and O'Neil found the water composition of all these sites to be similar in composition and reaction pathways for low-temperature based serpentinization rock-water reactions (Barnes & O'Neil, 1977). In 2012, Paukert et al., characterized the ionic makeup of spring and well water

samples from Samail ophiolite using ion chromatography (IC) on a Dionex 2000 with an AS18 column for the anions, and inductively coupled plasma atomic emission spectrometry (ICP-AES) with Horiba Jobin-Yvon Activa M with PFA nebulizer for the cations (Paukert et al., 2012). The resulting geochemistry of waters were classified as being of two different types: those that were high in the Mg^{2+} and $-HCO_3^-$ (named Type I waters), and those with high Ca^{+2} and $-OH^-$ (named Type II waters).

The serpentine soils are unique as they are naturally deprived in nutrients that plants need; instead they are rich in Mg, Fe, and trace elements that include Ni, Cr, Cd, Co, Cu, and Mn (Wildman et al., 1968, D'Amico & Previtali, 2012). This creates a challenging environment for plants to grow in. The serpentine endemic species are visibly different from other plants growing in a landscape with serpentine soil exposures and have evolved and shown adaptations that fit this unique environment (Safford et al., 2005; Alexander, 2007). Due to their harsh nature, the serpentine soils at Coast Range locale and other similar sites have been studied from an ecological point of view. How they weather under natural environments is little studied as yet. Also, the weathering processes tend to differ site to site due to differences in topography, parent rock mineralogy, climate and rainfall.

It is proposed that CRO is a site of on-going low temperature serpentinization leading to production of different fluids that are reflective of rock-water interactions. A reaction pathway can be modeled to explain the temporal changes in mineralogy and fluid chemistries. To confirm this, water samples were collected from Coast Range ophiolite, McLaughlin Natural Reserve area. The key environmental parameters were recorded onsite and the ionic makeup of the waters were determined

using ion chromatography (IC) for the concentrations of major anions (F^-, Cl^-, SO_4^{-2}, NO_3^-), and Inductively Coupled Plasma Atomic Emission Spectrometer system (ICP-AES) for major cations (Ca^{+2}, Na^+, Mg^{+2}, K^+). The ionic data were quantified and analyzed. JMP Statistical Data Analysis Software was used for principal components analysis (PCA) to explain key factors and processes controlling the water chemistries at CRO. X-ray diffraction (XRD) data from CRO well cores and ionic make up of four types of waters (local meteoric water, seawater, a 10% dilute seawater, and an ultrabasic groundwater solution) were added as an input in Geochemist's Workbench (GWB) software to model the evolving water chemistry, mineralogy, pH and Eh changes. As the terrestrial sites of serpentinization experience low temperature, relatively oxidizing weathering near the planetary surface, the aqueous geochemistry of waters and the corresponding mineral lithologies evolve and provide insight into the complex rock-water interactions.

GEOLOGIC SETTING

During the Jurassic and Cretaceous periods, the oceanic Farallon Plate, moving west, collided with the North American continental margin and underwent subduction. This subduction lead to the formation of the Coast Ranges and Sierra Nevada on the west coast of United States. With time, the scraping off of material from the down-going Farallon plate formed an accretionary wedge, known now as the Franciscan mélange (French for “mixture”), and the weathering of the Sierra Nevada settled in the ocean basin just beyond the tip of continent and became known as the Great Valley Sequence. Later, complex folding and faulting events between the two plates exposed a piece of the Middle Jurassic oceanic crust and mantle (ophiolite) named Coast Range Ophiolite, which has the Great Valley Sequence on the east, and the Franciscan complex on the west. The Coast Range Ophiolite consists largely of serpentinite, partly serpentinized peridotite, gabbro, and basalt (University of California, 2003).

FIELD SITE

About 600 km north of the Golden Gate Bridge is one block of the Coast Range Ophiolite, in the McLaughlin Natural Reserve, near the junction of Napa, Lake, and Yolo Counties. This unique geologic area of 6,940 acres is managed by the University of California to protect and conduct research in the unusual serpentine-rich habitats. In 2011, eight monitoring wells were installed, funded by the NASA Astrobiology Institute, in ultramafic units rich in serpentine minerals, derived from the regionally important convergent margin mélange environment. The CRO monitoring wells at the McLaughlin Natural Reserve provide a means to sample periodically the formation waters moving through a shallowly emplaced ultramafic unit, with logistically simple access.

Climate

The reserve receives an average precipitation of 75.7 cm per year, with the average temperatures of July as 24.6 ºC and January's average temperature of 7.3 ºC (Natural Reserve System University of California, 2018). Regional climate is Mediterranean-type, with summers being dry and hot, and winters wet and cold (Mathany & Belitz, 2015).

Hydrogeology

The movement of groundwater follows the area's topography and the direction of flow of the surface water features. The recharge to groundwater is primarily through the precipitation and runoff from surface water features (Mathany & Belitz, 2015).

Sampling Locations

Eight monitoring wells were installed near Lower Lake, CA, in the McLaughlin Natural Reserve. Wells were installed at two sites in the Reserve, namely the Quarry Valley and the Core Shed. These wells are designated (bottom of hole depth in meters provided in brackets after well ID): QV1-1 [23 m], QV1-2 [14.9 m], QV1-3 [34.6 m], CSW1-1 [19.5 m], CSW1-2 [19.2 m], CSW1-3 [23.2 m], CSW1-4 [8.8 m], CSW1-5 [27.4 m]. An old well known as Old Core Shed well, OCSW [82 m] is present near the Core Shed wells. This deep well was already present on site before the other wells were drilled. The main well for Core Shed wells is the CSW1-1, with the other Core Shed wells located within 5m of CSW1-1. The main well for the Quarry Valley wells is the QV1-1, with the other Quarry Valley wells present within 3m of QV1-1. Each well reaches a different depth in the shallow subsurface.

The two other sampling sites (TC1 and TC2) include an upstream and downstream point along a seasonally active ground-water fed creek, the Temptation Creek (TC). TC1 is the area where the groundwater seep is emerging from, and TC2 is the percolating water before it disperses into the landscape. The distance between TC1 and TC2 is about 515m with a relief of 65m (Figure 3).

ANALYTICAL METHODS

Field Methods

Collection of Water Samples

Water samples were collected during the months of May and June of 2016 and of 2017. The sampling sites included the 8 groundwater wells (CSW1-1, CSW1-2, CSW1-3, CSW1-4, CSW1-5), the Old Core Shed well (OCSW), and two surface water sites, Temptation Creek 1 (TC1) and Temptation Creek 2 (TC2).
Samples were collected via syringes (rinsed three times) fitted with 0.22 µm pore size filters. No pretreatment was required for IC samples, which were stored in clean, plastic laboratory bottles and frozen until analysis. The samples for ICP-AES were collected in certified 100 ml Nalgene bottles, spiked with 70% trace metal grade HNO_3, such that after sample addition, the solution concentration was ~2% HNO_3. Samples were chilled and transported to University of Rhode Island.

Collection of Field Data

Using the pre-installed bladder pumps manufactured by Geotech Environmental (Geotech Environmental Equipment, Inc., 2018) in each well, the waters were pumped into a flow through cell connected to a YSI-556 multiprobe that measures real time changes in chemical parameters observed during pumping. The environmental parameters noted on site were the pH, temperature (°C), conductivity (EC, in mS/cm), dissolved oxygen (DO, in mg/L), and oxidation reduction potential (ORP, in mV, corrected to Eh by addition of 200 mV to the value observed in the field).

Laboratory Methods

Anion and Cation Stock Standard Solutions

Certified and concentrated standard solutions of 50 mL Dionex™ Combined Six Cation Standard-I, (Lithium 50mg/L; Sodium 200mg/L; Ammonium 400mg/L; Potassium 200mg/L; Magnesium 200mg/L; Calcium 1000mg/L), and 50 mL Dionex™ Combined Seven Anion Standard I, (Fluoride 20mg/L; Chloride 30mg/L; Nitrite 100mg/L; Bromide 100mg/L; Nitrate 100mg/L; Phosphate 150mg/L; Sulfate 150mg/L) were purchased through Fisher Scientific. The Dionex™ standards for each individual ion were also obtained. The Stock solution standards were prepared using the deionized water from Thermo Scientific Barnstead T11 NANO PURE SYSTEM (ThermoFisher Scientific, n.d.) with the resistivity of 18.2 MΩ-cm @25˚C. Stock Standard solutions were stored at 4 ^{0}C in plastic bottles and protected from light. The same sourced deionized water was used throughout the sample analyses.

Titration of Samples

Small quantities from each collected sample were used to test for their chloride concentrations using HACH chloride test kit. It was vital that the samples with higher ion concentrations be diluted enough so that all the ions in sample would be in the detection range of the IC instrument.

Calibration standards

The calibration standards for each ion were prepared based upon the chloride concentration levels and the expected high and low detection limits of the ions in the water samples by serially diluting stock solutions for use in constructing the calibration curve in IC and ICP-AES (Table A-1).

Eluent Solution

The DX-500 IC requires the eluents 0.5 M sodium bicarbonate, 0.5M sodium carbonate, and 05M sodium bicarbonate-sodium carbonate eluent.

Sample preparation

Samples were individually diluted based upon their titration results and their expected ionic detection limits. For IC, samples were diluted as a solution of 1:10, 1:100, 1:1000, or no dilution was done. For ICP-AES, two sets were prepared. Set one contained all the non-diluted samples. Set two was diluted as 1:10, prepared by taking 5mL of sample and adding 45 mL of 2% HNO_3 to reach a final volume of 50mL in falcon tubes. Samples were diluted as per the protocol in appendix (Table A-2) and taken to the Brown University laboratory for anion and cation analysis. Samples were allowed to equilibrate to room temperature before analysis.

Procedural Lab Blanks

a) Blank preparation for IC:

IC procedural blanks were prepared by taking two 60 mL syringes, filled with deionized water. They were flushed three times, and then, for the fourth time, filled while attached with a Millipore Sterivex syringe-filter (22µm pore size) and emptied into 50 mL falcon tubes. Two falcon tubes were prepared for use as blanks.

b) Blank preparation for ICP-AES:

Two 60 mL syringes were each filled with 20 mL of 2% HNO_3. Syringe were covered at end with thumb and rotated to agitate the syringes so that both were all agitated inside with the 2% HNO_3. The 2% HNO_3 was drained, and procedure was

repeated three times. The fourth time, syringes were filled with 50 mL of 2% HNO_3. Two of these were prepared for use as blanks.

Quality Controls

In addition to the standards prepared, the IC and ICP-AES used internal check standards different from the calibration standards. For IC the FAS1, and for ICP-AES QC28 were used, both available from Inorganic Vendors. FAS1 is a 5-anion standard (Fluoride 0.2mg/L; Chloride 0.3mg/L; Nitrate 1mg/L; Phosphate 1.50mg/L; Sulfate 1.5mg/L), that is now sold as FAS 1A as a 7-anion standard (additional Bromide 1mg/L; and Nitrite 1mg/L).

The QC28 (Quality Control Standard 28) is a 125mL certified reference material set in a nitric acid / hydrofluoric acid matrix for stability. It is a multi-analyte custom made solution (Al, As, Be, Cr, Cd, Cu, Pb, Mg, Mo, K, Na, Tl, V, Sb, Ba, B, Ca, Co, Fe, Li, Mn, Ni, Se, Ag, Sr, Ti, Zn as 1mg/L and Si as 0.5mg/L).

Instrumentation

Dionex Modular DX 500 Ion Chromatography system

The detection of anions (F^-, Cl^-, SO_4^{-2}, NO_3^-) was done by measuring the conductivity of the separated anions as they eluted from the separation column based upon their affinity with the ion exchange column in the IC. The water samples were analyzed for their anion makeup by the use of Dionex Modular DX 500 Ion Chromatography system at the Brown University, Providence. The samples were prepared as two sets. Set one was non-diluted but filtered for removal of chloride. The samples were filtered for chlorine by running through the Fisher Scientific silver cartridges. Set two was diluted as per the dilution protocol per each sample. The

anions present were identified by their retention times, and their quantities were determined by the area of their peaks. The determination of peak parameters (area, height, retention time) was done using Dionex software. The samples were from 9 wells: OCSW, CSW 1-1, CSW 1-2, CSW 1-3, CSW 1-4, CSW 1-5, QV 1-1, QV 1-2, QV 1-3, and two were from a surface water creek site: TC1 and TC2.

Thermo Scientific iCAP 7400 Duo Inductively Coupled Plasma Atomic Emission Spectrometer system

The well water samples were analyzed for their cation makeup (Ca^{+2}, Na^{+}, Mg^{+2}, K^{+}) by the use of Thermo Scientific iCAP 7400 Duo Inductively Coupled Plasma Atomic Emission Spectrometer system at the Brown University, Providence. An ICP-AES system is made up of two parts: the inductively coupled plasma source, and the atomic emission spectrometry detector. The principal behind the working of ICP AES is the excitation of the samples as electrons, which emit energy at a diagnostic wavelength as they return to their ground states. The emitted energy is characteristic of each element and the intensity of energy is proportional to the concentration of that element. This method identifies the elemental wavelength, and their intensities, the ionic composition can be identified and quantified, relative to a standard. For ICP-AES analysis, the samples were prepared as two sets: Set one was non-diluted. Set two was diluted as 1:10. A total of 11 collected samples were tested for their cation composition, namely Old Core Shed Well (OCSW), Core Shed Wells (CSW 1-1, CSW 1-2, CSW 1-3, CSW 1-4, CSW 1-5), Quarry wells (QV 1-1, QV 1-2, QV 1-3), Temptation Creek (TC1, TC2).

Data Analysis

Principal Components Analysis

JMP Statistical Data Analysis Software (JMP version 10) was used to explain key factors and processes controlling the water chemistries at Coast Range Ophiolite. Water chemistry data and related environmental parameters (with exception of depth) were entered for multivariate statistical analysis and subjected to correlation matrix. Eigenvalue Pareto Plot, Score Plot, and Loading Plot were generated to extract information on the correlating factors.

Geochemist's Workbench

Geochemist's Workbench (GWB) REACT mode was used to model the low temperature alteration of a serpentinization-influenced water package passing through serpentinite host rock environment. React mode is a program in GWB that models and simulates reactions taking takes in a geochemical system. The REACT mode can trace the evolution of a system as it undergoes reactions in open and closed systems, under various defined conditions.

The conceptual model of the REACT mode simulation is shown in Figure 4 (Bethke & Yeakel, 2015). An initial system is defined, and then the REACT program calculates the system's initial equilibrium state. The program then simulates a reaction path by adding or removing reactants and adjusting the reaction conditions accordingly. The results are generated as an output dataset and calculations are broken down in a tabular form. REACT works by using the built-in rate laws for different reactions (mineral dissolution and precipitation; aqueous and surface complex dissociation and association; redox; microbially mediated reactions; gas transfers).

The inputs used in GWB modeling are shown in Table 1, Table 2 and Table 3. Minerals including antigorite, magnetite, greenalite react with four types of input waters (seawater, 10% dilution of seawater, local meteoric water, ultrabasic groundwater). The system is water-dominated, simulating reactions taking place about 1 to 3 meters below land surface at CRO.

RESULTS

The water samples collected at CRO are from nine wells, contextualized by one nearby groundwater-fed alkaline seep (Temptation Creek, TC), from which high elevation (TC1) and low elevation (TC2) samples were obtained. The three Quarry Valley wells (QV1-1, QV1-2, QV1-3) and six Core Shed wells (OCSW, CSW1-1, CSW1-2, CSW1-3, CSW1-4, CSW1-5) sample from different depths in peridotite bedrock at CRO (Figure 5) The QV wells are all within 3m of the main QV1-1 well, from which rock cores were obtained. The CSW wells are within 5m of the main CSW1-1 well, which also produced cores.

The key environmental parameters collected at CRO are shown in Table 4. The environmental parameters noted on site were the pH, temperature (°C), conductivity (EC, in mS/cm), dissolved oxygen (DO, in mg/L), and oxidation reduction potential (ORP, in mV, corrected to Eh by addition of 200 mV to the value observed in the field). The concentrations for major anions and cations are expressed as mg/L in Table 5.

The Ca/Mg ratios for TC1, TC2 and CSW1-4 are <1, dominated by Mg^{+2}; while the rest of the wells (OCSW, CSW1-1, CSW1-2, CSW1-3, CSW1-5, QV1-1, QV1-2, QV1-3) are >1, dominated by Ca^{+2} (Figure 6).

The high Ca^{+2} and Mg^{+2} concentration values for all the CRO samples can be seen in the Figure 7.

Another notable ionic composition of the CRO waters is their extremely high Na^+ and Cl^- concentrations (Figure 8). The Na^+ and Cl^- concentration overload is many times higher than that of the seawater.

When the individual Na^+ and Cl^- concentration cross-plot is graphed for the CRO samples and seawater, with the trendline passing through the SW, it can be seen that the Na/Cl ratio is low for QV1-1, CSW1-5, OCSW and high for QV1-3, CSW1-1, whereas the remaining wells QV1-2, CSW1-2, CSW1-3, CSW1-4 appear to be dilutions of seawater as they remain very close on the seawater trendline (Figure 9). If the increased Na drives these ratios up, there is possible Na desorption from clays or albite dissolution, however if the low Na drives these ratios down, there may be albitization of altered mafic (CSW site) or Na-sorption in the new smectite group clays.

In Figure 9, the OCSW well, shows the most deviation in the Na^+ and Cl^- content from the rest of the wells, being extremely high in Na^+ as well as in Cl^- concentrations (Na^+=1822ppm, Cl^-=4041ppm).

Regarding the ratio of total Na^+ ion content versus total Cl^- ions, all the well samples contain more Cl^- ions than Na^+ ions, which is the case for seawater's Na^+ and Cl^- content. An exception of this is present for the sole well CSW1-1 (Na^+ =312.8ppm, Cl^-=113.6 ppm). Here, Na^+ concentration is higher than Cl^-. The order of wells from most to least is OCSW> CSW1-3> CSW1-5> CSW1-2> QV1-5> QV1-2> QV1-3> CSW1-4> CSW1-1. The briniest OCSW is the deepest well (82m). The least saline is CSW1-1 (the sole well with more Na^+ than Cl^-), and second-from-least-saline CSW1-4 is the shallowest well (8.8m) in the entire set of monitoring wells. The

proximity of the CSW1-1 to CSW1-2 is also of interest as not only are the two wells close to each other but are also of very similar depths (CSW1-1=19.5m, CSW1-2=19.2m), yet where the CSW1-2 is the fourth most saline one (with similar Na^+/Cl^- ratio to that of the seawater), but CSW1-1 is the least saline of all. Overall, the Core Shed Valley wells are brinier than the Quarry Valley wells (with the exception of CSW1-1, and least deep CSW1-4).

The in-field temperature measurements of the samples show the highest temperature bearing well as the OCSW (17.81^0C), with the QV1-2 (17.35^0C) being very close to the OCSW. Though the OCSW is the deepest and warmest in temperature, the data for other wells and springs show no correlation between the temperature and depth. Overall, the temperature range very close for the CSW and QV wells (between 15-17^0C), and the temperatures for the TC1 and TC2 are on slightly lower side of ~ 13-14^0C.

The deepest OCSW has the highest electrical conductivity (EC) of 11.44 mS/cm, and the shallowest CSW1-4 has the least EC reading of only 1.86 mS/cm, though no direct relation is seen for the EC and depth in the other wells (Figure 10). With the exception of the OCSW (deepest) and CSW1-4 (shallowest), the CSW wells are ~5mS/cm in range, the QV wells are on slightly lower EC range of ~4mS/cm, and TC1 and TC2 both show almost the same EC of ~3mS/cm.

The dissolved oxygen (DO) is highest for the shallowest well CSW1-4 (19.5% DO), while its neighboring well CSW1-3 has the lowest DO of 0.7%. The range for QV wells for DO is ~2-5%, and ~1-2% DO for CSW wells and the TC springs. There

is no apparent relationship of DO% with bottom of well depth; though the shallowest well (CSW1-4) does reflect the greatest well DO reading of 19.5%.

The Eh values range from +418mV (TC1) to -110mV (CSW1-1). Using Garrels and Christ (1965) plot that shows the Eh-pH relation of waters of various natural environments, OCSW, CSW1-1, and CSW1-5 plot at pH of between 10-14, with very negative Eh values, plotting within natural environments that are isolated from the atmosphere. TC1 and TC2 plot around pH 8, with positive Eh values, signalling environments in contact with the atmosphere (Figure 11).

The pH ranges for samples are from 13.5 to 7.6 in the following order: CSW1-1> QV1-1> CSW1-3> OCSW> CSW1-5> QV1-3> QV1-2> CSW1-2> TC2> TC1. The highest pH well CSW1-1 has the lowest Eh value, while the lowest pH site TC1 has the highest Eh value; however, no linearity exists between the other samples.

The graphs for EC (as a proxy for total dissolved solids) and ionic concentrations for CRO show similar curve profiles for both, except for CSW1-1 (Figure 12). The unique ionic composition and concentrations that makes CSW1-1 differ from other CRO wells, can further be seen in the Stiff diagrams of the samples created in the GWB (Figure 13). The Stiff diagram for OCSW is most unique among the CRO samples, followed only by CSW1-1. The CSW1-2, CSW1-4, and QV1-2, show similar ionic compositions, though the concentrations seem to shift amongst the samples, while maintaining the same overall Stiff diagram features. The Stiff diagrams for TC1 and TC2 are very closely related with each other, showing more ionic concentration of the same makeup present in TC1, than for TC2.

Overall, the ionic concentrations of all the CRO samples, MW and SW show that the CRO samples distinguish themselves from other waters due to their extremely high Na^{+}- Cl^{-} concentrations, followed by the high Mg^{+2} and Ca^{+2} concentrations. The complete concentration range of all the anions and cations can be seen in Figure 14.

The principal components analysis shows that the first two principal components together account for 64.4% (41+23.4=64.4) of the total variation in the data. The 1st component (PC1) accounts for 41% of the variation, and the 2nd component (PC2) accounts for 23.4% of the variation in the data set (Figure 15).

The Loading Plot shows that if divided vertically into two equal halves, the right half side shows factors that are positively correlated to the 1st component. These factors include Ca^{+2}, K^{+}, NO_3^{-}, Mg^{+2}, and F^{-}. The left half side includes factors that are negatively correlated to the 1st component. These include DO, SO_4^{-2}, pH, temperature, conductivity, Na^{+} and Cl^{-}. The top right quadrant (I) containing Ca^{+2}, K^{+}, NO_3^{-}, Mg^{+2} show positive correlations with 2nd component (and are also positively correlated with the 1st component). The lower right quadrant (IV) containing F^{-} shows the negative correlation with the 2nd and positive with the 1st component. The top left quadrant (II) containing pH, temperature, conductivity, Na^{+} and Cl^{-} show negative correlation with 1st and positive correlation to the 2nd component. Similarly, the lower left quadrant (III) containing DO and SO_4^{-2} show negative correlation to 1st as well as 2nd component.

The scatter plot representation of the first two principal components can be seen in the Score Plot. Here, the triangles represent the Temptation Creek, circles are the Core Shed Wells, and the squares are the Quarry Valley Wells. Temptation Creek

data for both sites (TC1, TC2) lies in quadrant I, showing positive correlation with first and second components in regards to Ca^{+2}, Mg^{+2}, K^{+}, and NO_3^{-}. The majority of the clustering is within the quadrant III which shows the negative correlation of 1st and 2nd components in regards to their DO and SO_4^{-2} content. The OCSW is plotted as being the furthest from all the data points (quadrant II). Therefore, the OCSW shows a marginal difference in Na^{+}, Cl^{-}, conductivity, temperature, and pH from all the rest of the water samples. The correlations data table is provided in the (Table 6).

The GWB software was used to simulate the possible reaction pathways using the input minerals from X-ray diffraction (XRD) profiles of the cores taken from CRO (Cardace et al., 2013) with four types of water inputs (seawater, 10% dilute seawater, local meteoric water, ultrabasic groundwater). The minerals were made to react at three different temperatures (25^0C, 100^0C, 2^0C). The GWB software predicted the changes in pH, Eh, mineralogy, and in fluid chemistry as the serpentine-rich environment reacted with the different waters over a total time span of 100 million years (Ma). The software inputs are listed in Tables 1-3. It should be noted that for the ultrabasic groundwater reacting with serpentine, the system could only proceed to reach completion at the temperature of 25^0C. Under 100^0C the residual was too large, and at 2^0C the initial solution was too supersaturated to proceed.

Changes in pH at 25^0C:

In the case of the seawater reacting with serpentine, there is a small pH increase in the initial 15 Ma (starting from time= 0 Ma), however the system gains a stable pH soon and then stabilizes itself for the rest of the defined time period. In the case of the dilute seawater a very small pH increase occurs in the very beginning, however the pH drops

back to the original very soon and stays close to the starting pH for the rest of the time period. The model for meteoric water shows an impressive and sharp increase in pH immediately after the system starts to react. The high pH increase is achieved very quickly within the first few years and then the system stabilizes itself somewhat, with a very gradual increase over the 100 Ma. The model for the ultrabasic groundwater shows a high starting pH value that continuously keeps on decreasing with the passage of time. Even after 100 Ma, the system still maintains high pH values with no stabilization (Figure 16).

Changes in Eh at 25^0C:

The Eh models for seawater and dilute seawater show a steep and immediate decrease in values (reaching very high negative values) followed by stabilization within the first 10-15 Ma. The meteoric seawater shows a similar immediate drop in Eh, however the Eh drop reach extremely high negative values within the first 5 Ma. Starting from zero, the Eh value drops to negative 340, followed by brief stabilization and then dropping again to reach negative 400, and finally gaining somewhat stabilization for the remaining time period. The last model that includes the ultrabasic groundwater shows the most Eh variation over 100 Ma. It decreased to high negative values like the other three models, but unlike the others, the system struggles to gain stabilization. Even after 100 Ma, the system's redox potential is still changing (Figure 17).

Changes in fluid chemistry at 25^0C:

In the case of the seawater, notable shifts are seen in Al^{+++}, Fe^{++}, H^+, $SiO_2(aq)$ and HCO_3^- ions for the first 20 Ma. Al^{+++}, Fe^{++} increase, $SiO_2(aq)$ increase and then decrease, and H^+, and HCO_3 decrease. For the dilute seawater, a slight concentration

increase takes place for Al^{+++}, Fe^{++}, SiO_2 (aq) and H^+. The system attains stability within the first 10 Ma. The meteoric water shows different ionic fluctuations. Unlike the first two models, Fe^{++} drops but then reaches back to the same initial concentration within 20 Ma. H^+ shows increase in concentration as in the dilute seawater scenario, but with much steeper gradient and more quickly. Instead of Al^{+++}, SO_4^{--} shows a notable decline during the first 20 Ma, after which the water chemistries show no noticeable change. The ultrabasic groundwater shows the most evolved waters, that are still changing after 100 Ma. The changes involve leaching of ions that include Fe^{++}, SiO_2(aq) and HCO_3^- into the waters. The ions that decrease in the fluids are Al^{+++} and SO_4^{--}. Even after the 100 Ma, the waters are still reacting and evolving in this mode (Figure 18).

Changes in mineralogy at 25^0C:

The models for seawater show emergence of a few different minerals during the first 20 Ma. The mineral makeup after 100 Ma includes dolomite (carbonate mineral), saponite-Na (smectite group clay mineral), phlogopite (mica family of phyllosilicate), hematite (oxide mineral), pyrite (sulfide mineral), muscovite (hydrated phyllosilicate), phengite (mica group), quartz (oxide), Talc (silicate mineral) and the antigorite clays minerals. The mineral that shows the most significant increase in concentration is Hematite (within 10 Ma). Overall, antigorite is the most abundant mineral. The dilute seawater shows simpler mineralogy consisting of saponite-Mg (smectite group clay mineral), muscovite (hydrated phyllosilicate), hematite (oxide mineral), pyrite (sulfide mineral), gibbsite (aluminum hydroxide), and phlogopite (mica family of phyllosilicate), with emergence of Hematite after 10 Ma. The meteoric water shows

antigorite (most abundant), saponite-Mg, clinochl 14A (chlorite mineral), magnetite, hematite, Ripidolite 14A (chlorite mineral), and pyrite. Magnetite appears after 20 Ma, however Ripidolite 14A appears to be an indicator mineral as it appears after 80 Ma. The ultrabasic model shows most dynamic mineralogy with emergence of various minerals over the entire time period. Here, the notable minerals forming are magnetite (after ~40 Ma), FeO (~60 Ma) with the most recent one being annite (~90 Ma). The mineralogy at the end of 100 Ma includes presence of antigorite (most abundant), phlogopite, andradite (garnet group mineral), wollastonite (inosilicate mineral), clinochl 14A (chlorite group), diopside (inosilicate mineral), calcite (carbonate), hematite, magnetite, FeO, annite (phyllosilicate mineral of mica family), and pyrite (Figure 19).

pH variations among different temperature models:

The pH at 25^0C and 2^0C for seawater, dilute sea, and meteoric water (no ultrabasic water model present) show very similar patterns. All three types of waters show an initial increase in pH (dilute seawater pH drops down after the initial increase). However, the pH model at 100^0C show decreasing pH values for seawater and dilute seawater. In the case of the meteoric water model at 100^0C, it shows the same pH increase as seen in meteoric waters at 25^0C and 2^0C temperatures (Figure 16, 20,21).

Eh variations among different temperature models:

Like the pH patterns, the Eh at 25^0C and 2^0C for seawater, dilute sea, and meteoric water (no ultrabasic water model present) show very similar patterns. The seawater at 25^0C and 2^0C show same patterns of decrease in redox potential. The dilute seawaters of 25^0C and 2^0C also show similar behavior to each other. Likewise, the meteoric

waters at 25^0C and 2^0C show patterns identical to each other. All four types of waters at 25^0C and 2^0C, show trend of decreasing redox values, resulting in very reducing waters. In the case of the model for 100^0C, both the seawater and dilute seawater decrease in Eh values like the waters at 25^0C and 2^0C, however instead of gaining stability the values show increase before finally achieving stability. The behavior of meteoric water for 100^0C is the same as that of meteoric waters at 25^0C and 2^0C (Figure 17, 22, 23).

Fluid chemistry variations among different temperature models:

Like pH and Eh, the seawaters and the meteoric waters at 25^0C and 2^0C show similarities as the same ions undergo changes in similar ways, for both temperature models. The dilute seawater models for 25^0C and 2^0C are also similar to each other. However, at 100^0C, the seawater shows a different water chemistry with HCO_3^- and H^+ leaching into the waters, and Al^{+++} with an initial increase and then stabilizing. The meteoric water at 100^0C also behaved differently than that of other temperature models. SO_4^{--} concentrations remain higher in this model, and unlike the absence of H^+ under 25^0C and 2^0C, here H^+ is produced after 70 Ma (Figure 18, 24, 25).

Mineralogy variations among different temperature models:

The greatest variation due to temperature difference is present in the mineralogy of the models. The input minerals included antigorite, beidellite-Mg, brucite, clinochi-7A, greenalite, and magnetite. The seawater end products include antigorite, saponite-Na, dolomite, phlogopite, hematite, pyrite, muscovite, phengite, nontronite-Na, talc and quartz. No new minerals are forming beyond the first 15 Ma. In the case of 100^0C the mineralogy includes antigorite, dolomite, hematite, pyrite, brucite, saponite-Mg, and

clinochl 14A. New minerals are forming after 15 Ma. In the case of 2^0C, the end minerals are antigorite, saponite-Mg, clinochl 14A, hematite, pyrite, talc, saponite-Ca, with the emergence of Ripidolite 14A around 25 Ma. In the case of dilute seawater, 25^0C shows very simple mineralogy makeup consisting of saponite-Mg, hematite, pyrite, muscovite, phlogopite, and gibbsite. No antigorite is present. At the temperature of 100^0C, we see appearance of different minerals over time. It includes all the minerals of 25^0C (except phlogopite) and also additional ones that include amesite 14A, clinochl 14A, dolomite, and antigorite. The emergence of muscovite and gibbsite takes place after 40 Ma. At 2^0C, the mineralogy is simple like in 25^0C model, with the minerals saponite-Na, hematite, pyrite, muscovite, dolomite, and a different mineral nontronite-Na emerging after ~60 Ma. In the case of meteoric waters, all three temperature models include antigorite, saponite-Mg, clinochl 14A, magnetite, hematite, and pyrite. What sets these apart is the formation of Ripidolite 14A after 80 Ma (at 25^0C), absence of Ripidolite 14A (at 100^0C), and presence of talc and saponite-Ca (at 2^0C) (Figure 19, 26, 27).

DISCUSSION

The process of serpentinization leads to the formation of waters that are extremely rare in the natural environments (Neal, 1984; Chavagnac et al., 2013). The physical and chemical data from CRO shows the presence of Type I and Type II waters at CRO. The Ca/Mg ratios show that TC1, TC2 and CSW1-4 are Type I (high Mg^{+2}) open system waters. OCSW, CSW1-1, CSW1-3, and QV1-1 are the Type II (high Ca^{+2}) closed system water. CSW1-2, CSW1-5, QV1-2, and QV1-3 are found to be the intermediate, mixed water (Figure 28). CSW1-4, the shallowest of all the wells, is an open water system, unlike any other groundwater wells. High pH, high Ca^{+2}-OH^{-} waters, and lower pH, high Mg^{+2}-HCO_3^{-} waters are unique to serpentinizing sites (Barnes and O'Neil, 1969; Paukert et al., 2012).

All the samples show high Na^{+} and Cl^{-} concentrations. This is due to the reaction of Cretaceous seawater trapped within the ophiolite during its emplacement and reacting with the surrounding rocks (Peter, 1993; Schulte, 2006). The stable isotope data from CRO also supports presence of seawater as the serpentinizing fluid (Barnes et al., 2013). The OCSW shows the greatest Na^{+} and Cl^{-} concentration due to being the deepest with more surface area for interacting with altered fluids and bedrock constituents. CSW1-2, CSW1-3, CSW1-4, and QV1-2 show similar Na^{+} and Cl^{-} ratios as that of sea water, therefore they appear to be dilutions of varying extent of the trapped sea waters. These dilutions of SW can be due to the influx of meteoric and other shallowly sourced waters.

All the well samples maintain the same $Cl^- > Na^+$ content as in seawater, with the exception of CSW1-1. CSW wells are brinier than the QV wells. Despite the close proximity of all the CSW wells to each other, CSW 1-1 is least saline of all the wells, including the QV wells. One of the possible explanation that puts CSW1-1 apart from others might be a result of casing. All the wells except for CSW1-1 and QV1-1 were cased with PVC pipes. The CSW1-1 and QV1-1 are also larger in diameter than the other pipes (Twing et al., 2017).

Temperature profile of the wells show variations that are irrespective of the depth. The subtle temperature variations noted here are seasonal and site-specific (related to heat from solar radiation striking the land surface, conducted to some depth below the land surface), or in-flow of regional geothermal waters. Using Garrels and Christ's Eh-pH plot for finding the limits of the naturally occurring aqueous environments, OCSW, CSW1-1, and CSW1-5 show stability range within environments that are isolated from the atmosphere (Figure 29). These are the highly alkaline waters with strong reducing values. The two alkaline springs (TC1, TC2) are in the environment that are in contact with the atmosphere and thereby have the most oxidizing values, while still being slightly alkaline. The rest of the samples, CSW1-2, CSW1-3, CSW1-4, QV1-2, QV1-2, and QV1-3 show properties of transitional environments, and are in the spectrum of high alkaline waters. Overall, CSW groundwaters are more reducing than the QV ones. Based upon this data, a graphical representation showing observed bedrock-water interactions for the wells and spring waters, is proposed in Figure 30.

GWB software was used to predict the changes that took place over the 100 Ma time frame, using four kinds of input waters (seawater, 10% dilute seawater, meteoric

water, ultrabasic groundwater) and under three different temperature settings (2^{O}C, 25^{O}C, 100^{O}C). The GWB software showed no effect of temperature for 2^{O}C and 25^{O}C. In both models, the pH increases sharply for meteoric water, gradually for seawater, and a very small change in the case of dilute seawater. This is consistent with the observed high alkaline pH values for CRO as well as other known serpentinizing site. Similarly, the results for Eh showed no effect of temperature over Eh changes. All kinds of water, at all three temperatures, showed the decreasing (high negative) Eh values which are consistent with extremely reducing waters as observed in field at CRO and other serpentinizing sites. The software also showed leaching of minerals in and out of the water as it flows through the bedrock, with corresponding mineralogical changes in the serpentine rich environment. Leaching of the ultramafic rocks into the reacting waters is considered to be influenced by the chemical properties of water, the temperature, pressure, and the chloride content (Moody, 1976). The models for all the waters show that the leaching is lowest for 2^{O}C, with an increase for 25^{O}C, and the most leaching taking place at 100^{O}C. Study on Oman and Ligurian ophiolites show that the fluid compositions vary among one ophiolite to another, and also within the same ophiolite (Chavagnac et al., 2013).

The main ions that take place in noticeable chemical changes in waters are Al^{+++}, Fe^{++}, H^{+}, $SiO_2(aq)$, SO_4^{--} and HCO_3^{-}. Major changes are noted for the first 20 Ma, however the model for the ultrabasic groundwater show considerable changes throughout the 100 Ma. Generally, the concentrations of Al^{+++}, $SiO_2(aq)$, and Fe^{++} show leaching in as well as out of the waters over time. These ions provide explanation for corresponding mineralogical changes. The models for all three

temperatures show weathering of various minerals into their constituents, as well as appearance of characteristic new minerals over time. Model show antigorite as the most abundant serpentine mineral, which is a prograde metamorphism indicator (Moody, 1976). Numerous smectites, phyllosilicates, inosilicates are formed. Al^{+++} concentrations in fluids are explained by the emergence of albites (saponite-Na, muscovite, annite, gibbsite). This also provides the answer to the observed Na/Cl ratios in the CRO groundwaters (Figure 9). GWB modeling suggests that it must be the low Na that drove the Na/Cl ratio down due to albitization of altered mafic and/or Na-sorption in the new smectite group clays. Changes in observed Fe^{++} concentration in fluid waters can be the result of formation of hematite, pyrite, and magnetite. Annite (ultrabasic model at $25^{O}C$) appears to one of the marker minerals forming during the last 15 Ma (around ~85 Ma and onwards). Also, a smectite nontronite is formed in dilute seawater at $2^{O}C$ (as an apparent marker mineral, appearing ~60 Ma after start of serpentinization process) and seawater at $25^{O}C$. Nontronite (dioctahedral smectite) has been found on Mars surface by orbiting CRISM (Compact Reconnaissance Imaging Spectrometer for Mars) (Morris et al., 2010) and OMEGA (Observatoire pour la Mine´ralogie, l'Eau, les Glaces, et l'Activite) (Bibring, et al., 2005). Along with the smectite clay minerals, kaolinites have also been found at Mars (Baumeister et al., 2011). All the GWB models show the formation of antigorite, hematite, muscovite, pyrite, and saponite. The ultrabasic groundwater model ($25^{O}C$) show these same minerals along with emergence of some minerals unique to this system only. These include andradite, wollastonite, diopside, calcite, annite, and FeO(c). Andradite, wollastonite, diopside, and calcite contain Ca^{++}. Their presence only in the ultrabasic

model supports the presence of Ca^{++} in high alkaline, closed water systems (Type II). Also, FeO(c) formation is limited to highly reducing environment (highly alkaline, Type II). This is supported by the findings that Mg is completely depleted in waters of pH 10.5 and higher, whereas Ca^{++} accumulates with pH increase (Chavagnac, 2013).

Among all the GWB models, the most difficult model to predict fluid composition accuracy would be in the case of meteoric model because meteoric waters undergo unpredictable compositional changes during runoff.

CONCLUSION AND FUTURE WORK SUGGESTIONS

The Coast Range Ophiolite can be considered a site of ongoing low temperature serpentinization, with weathering related processes at work evidenced by environmental and geochemical parameters (redox measurements, temperature, pH, electrical conductivity, ionic composition). Physical parameters highlight that these high pH and low Eh groundwaters fall into known ranges for serpentinizing systems. The analytical chemistry confirms presence of different fluids that are reflective of rock-water interactions. Ca^{+2}-OH^{-} and Mg^{+2}-HCO_3^{-} waters are present and still evolving. Use of the Geochemist's Workbench provides insight into the changing fluid chemistry and corresponding mineralogical changes in the bedrock. The software further identifies the weathering profiles and appearance of indicator minerals (*e.g.*, smectites, albites, chlorites) that not only reflect the weathered stage of post-serpentinization, but also help in identification of serpentinizing terranes on Mars and other serpentinization-related celestial bodies (*e.g.*, Europa, Enceladus) in our Solar System and beyond.

Future works are suggested in collection of soil samples from Coast Range ophiolite and tested for modeling accuracy. The software Geochemist's Workbench did not allow for biological inputs, which are also an important aspect to consider in water-rock reactions. Furthermore, the local rain samples' isotope data can provide us with more detailed insight into the complex weathering of serpentinites.

REFERENCES

Alexander, E. B., Coleman, R. G., Harrison, S. P., & Keeler-Wolfe, T. (2007). *Serpentine geoecology of western North America: geology, soils, and vegetation*. OUP USA.

Allen, D. E., & Seyfried Jr, W. E. (2004). Serpentinization and heat generation: constraints from Lost City and Rainbow hydrothermal systems1. *Geochimica et Cosmochimica Acta*, *68*(6), 1347-1354.

Alt, J. C., Schwarzenbach, E. M., Früh-Green, G. L., Shanks III, W. C., Bernasconi, S. M., Garrido, C. J., & Marchesi, C., (2013). The role of serpentinites in cycling of carbon and sulfur: seafloor serpentinization and subduction metamorphism. *Lithos*, *178*, 40-54.

Andreani, M., Luquot, L., Gouze, P., Godard, M., Hoise, E., & Gibert, B. (2009). Experimental study of carbon sequestration reactions controlled by the percolation of CO2-rich brine through peridotites. *Environmental Science & Technology*, *43*(4), 1226-1231.

Barnes, I., & O'Neil, J. R. (1969). The relationship between fluids in some fresh alpine-type ultramafics and possible modern serpentinization, western United States. *Geological Society of America Bulletin*, *80*(10), 1947-1960.

Barnes, I., LaMarche, V. C., & Himmelberg, G. (1967). Geochemical evidence of present-day serpentinization. *Science*, *156*(3776), 830-832.

Barnes, I., O'Neil, J. R., & Trescases, J. J. (1977). Present day serpentinization in New Caledonia, Oman and Yugoslavia. *Geochimica et Cosmochimica Acta*, *42*(1), 144-145.

Barnes, I., Rapp, J. B., O'Neil, J. R., Sheppard, R. A., & Gude, A. J. (1972). Metamorphic assemblages and the direction of flow of metamorphic fluids in four instances of serpentinization. *Contributions to Mineralogy and Petrology*, *35*(3), 263-276.

Barnes, J. D., Eldam, R., Lee, C. T. A., Errico, J. C., Loewy, S., & Cisneros, M. (2013). Petrogenesis of serpentinites from the Franciscan Complex, western California, USA. *Lithos*, *178*, 143-157.

Berner, E. K., & Berner, R. A. (1987). *Global water cycle: geochemistry and environment*. Prentice-Hall.

Bethke, C. M., & Yeakel, S. (2015). The Geochemist's Workbench (Version 10.0): Reaction modeling guide. *Aqueous Solutions, LLC, Champaign, Ill*.

Bibring, J. P., Langevin, Y., Gendrin, A., Gondet, B., Poulet, F., Berthé, M., ... & Drossart, P. (2005). Mars surface diversity as revealed by the OMEGA/Mars Express observations. *Science*.

Blank, J. G., Green, S. J., Blake, D., Valley, J. W., Kita, N. T., Treiman, A., & Dobson, P. F. (2009). An alkaline spring system within the Del Puerto Ophiolite (California, USA): a Mars analog site. *Planetary and Space Science*, *57*(5), 533-540.

Burns, S. J., & Matter, A. (1995). Geochemistry of carbonate cements in surficial alluvial conglomerates and their paleoclimatic implications, Sultanate of Oman. *Journal of Sedimentary Research*, *65*(1).

Cardace, D., Hoehler, T., McCollom, T., Schrenk, M., Carnevale, D., Kubo, M., and Twing, K. 2013. Establishment of the Coast Range ophiolite microbial observatory (CROMO): drilling objectives and preliminary outcome. *Scientific Drilling*, 16: 45–55, www.sci-dril.net/16/45/2013/ doi:10.5194/sd-16-45-2013.

Cardace, D., Hoehler, T. M., McCollom, T. M., Schrenk, M. O., & Kubo, M. D. (2014). Integration of 3 Consecutive Years of Aqueous Geochemistry Monitoring Serpentinization at the Coast Range Ophiolite Microbial Observatory (CROMO), Northern California, USA. In *AGU Fall Meeting Abstracts* (Vol. 1, p. 4835).

Chavagnac, V., Monnin, C., Ceuleneer, G., Boulart, C., & Hoareau, G. (2013). Characterization of hyperalkaline fluids produced by low-temperature serpentinization of mantle peridotites in the Oman and Ligurian ophiolites. *Geochemistry, Geophysics, Geosystems*, *14*(7), 2496-2522.

Chizmeshya, A. V., McKelvy, M. J., Squires, K., Carpenter, R. W., & Bearat, H. (2007). *A novel approach to mineral carbonation: Enhancing carbonation while avoiding mineral pretreatment process cost*. Arizona State University.

Choi, S. H., Shervais, J. W., & Mukasa, S. B. (2008). Supra-subduction and abyssal mantle peridotites of the Coast Range Ophiolite, California. *Contributions to Mineralogy and Petrology*, *156*(5), 551

Corliss, J. B., Baross, J. A., & Hoffman, S. E. (1981). A hypothesis concerning the relationships between submarine hot springs and the origin of life on earth. *Oceanologica Acta, Special issue*.

D'Amico, M. E., & Previtali, F. (2012). Edaphic influences of ophiolitic substrates on vegetation in the Western Italian Alps. *Plant and soil*, *351*(1-2), 73-95.

Dickinson, W. R., Hopson, C. A., Saleeby, J. B., Schweickert, R. A., Ingersoll, R. V.,

Pessagno Jr, E. A., & Munoz, I. M. (1996). Alternate origins of the Coast Range ophiolite (California): Introduction and implications. *GSA today*, *6*(2), 1-10.

Ehlmann, B. L., Mustard, J. F., & Murchie, S. L. (2010). Geologic setting of serpentine deposits on Mars. *Geophysical research letters*, *37*(6).

Etiope, G. (2017). Abiotic methane in continental serpentinization sites: an overview. *Procedia Earth and Planetary Science*, *17*, 9-12.

Garrels, R. M., and Christ, C. L., 1965, Solutions, minerals, and equilibria: San Francisco, California, Freeman, Cooper & Company, 450 p.

Geotech Environmental Equipment, Inc. (2018). Geotech Bladder Pumps: Installation and Operation Manual. Retrieved January 10, 2017, from http://www.geotechenv.com/Manuals/Geotech_Bladder_Pumps.pdf

Hill, S. J. (Ed.). (2008). *Inductively coupled plasma spectrometry and its applications* (Vol. 8). John Wiley & Sons.

Kelemen, P. B., Matter, J., Streit, E. E., Rudge, J. F., Curry, W. B., & Blusztajn, J. (2011). Rates and mechanisms of mineral carbonation in peridotite: natural processes and recipes for enhanced, in situ CO2 capture and storage. *Annual Review of Earth and Planetary Sciences*, *39*, 545-576.

Lang, S. Q., Butterfield, D. A., Schulte, M., Kelley, D. S., & Lilley, M. D. (2010). Elevated concentrations of formate, acetate and dissolved organic carbon found at the Lost City hydrothermal field. *Geochimica et Cosmochimica Acta*, *74*(3), 941-952.

Martin, W., Baross, J., Kelley, D., & Russell, M. J. (2008). Hydrothermal vents and the origin of life. *Nature Reviews Microbiology*, *6*(11), 805.

Mathany, T.M., and Belitz, K. (2015). Groundwater quality in the Northern Coast Ranges Groundwater Basins, California: U.S. Geological Survey Fact Sheet 2014–3114, 4 p., https://dx.doi.org/10.3133/fs20143114.

Moody, J. B. (1976). Serpentinization: a review. *Lithos*, *9*(2), 125-138.

Morris, R. V., Ming, D. W., Golden, D. C., Graff, T. G., & Achilles, C. N. (2010, March). Evidence for interlayer collapse of nontronite on Mars from laboratory visible and near-IR reflectance spectra. In *Lunar and Planetary Science Conference* (Vol. 41, p. 2156).

Natural Reserve System University of California (2018). McLaughlin Natural

Reserve. Retrieved January 12, 2017, from https://ucnrs.org/reserves/mclaughlin-natural-reserve/

Neal, C., & Stanger, G. (1983). Hydrogen generation from mantle source rocks in Oman. *Earth and Planetary Science Letters*, *66*, 315-320.

Neal, C., & Stanger, G. (1984). Calcium and magnesium hydroxide precipitation from alkaline groundwaters in Oman, and their significance to the process of serpentinization. *Mineralogical Magazine*, *48*(347), 237-241.

Paukert, A. N., Matter, J. M., Kelemen, P. B., Shock, E. L., & Havig, J. R. (2012). Reaction path modeling of enhanced in situ CO 2 mineralization for carbon sequestration in the peridotite of the Samail Ophiolite, Sultanate of Oman. *Chemical geology*, *330*, 86-100.

Peters, E. K. (1993). D-18O enriched waters of the Coast Range Mountains, northern California: Connate and ore-forming fluids. *Geochimica et Cosmochimica Acta*, *57*(5), 1093-1104.

Russell, M. J. (2007). The alkaline solution to the emergence of life: energy, entropy and early evolution. *Acta biotheoretica*, *55*(2), 133-179.

Safford, H. D., Viers, J. H., & Harrison, S. P. (2005). Serpentine endemism in the California flora: a database of serpentine affinity. *Madroño*, *52*(4), 222-257.

Salhi, E., & Von Gunten, U. (1999). Simultaneous determination of bromide, bromate and nitrite in low μg l− 1 levels by ion chromatography without sample pretreatment. *Water Research*, *33*(15), 3239-3244.

Schulte, M., Blake, D., Hoehler, T., & McCollum, T. H. O. M. A. S. (2006). Serpentinization and its implications for life on the early Earth and Mars. *Astrobiology*, *6*(2), 364-376.

Szponar, N., Brazelton, W. J., Schrenk, M. O., Bower, D. M., Steele, A., & Morrill, P. L. (2013). Geochemistry of a continental site of serpentinization, the Tablelands Ophiolite, Gros Morne National Park: a Mars analogue. *Icarus*, *224*(2), 286-296.

ThermoFisher Scientific. (n.d.). *Thermo Scientific™ Barnstead™ Nanopure™ Accessories and Consumables.* Retrieved August 13, 2017, from https://www.thermofisher.com/order/catalog/product/D50280.

Tu, V., Baumeister, J., Metcalf, R., Olsen, A., & Hausrath, E. (2011). Serpentinite weathering and implications for Mars.

Twing, K. I., Brazelton, W. J., Kubo, M. D., Hyer, A. J., Cardace, D., Hoehler, T. M.,

... & Schrenk, M. O. (2017). Serpentinization-influenced groundwater harbors extremely low diversity microbial communities adapted to high pH. *Frontiers in microbiology*, *8*, 308.

University of California, Davis. (2003). *Natural history of the McLaughlin Reserve: Napa, Lake and Yolo counties California*. Davis, Calif: University of California, Natural Reserve System. Retrieved September 22, 2017, from https://naturalreserves.ucdavis.edu/sites/g/files/dgvnsk1091/files/inline-files/MCL_geology.pdf

Wildman, W. E., Jackson, M. L., & Whittig, L. D. (1968). Iron-Rich Montmorillonite Formation in Soils Derived from Serpentinite 1. *Soil Science Society of America Journal*, *32*(6), 787-794.

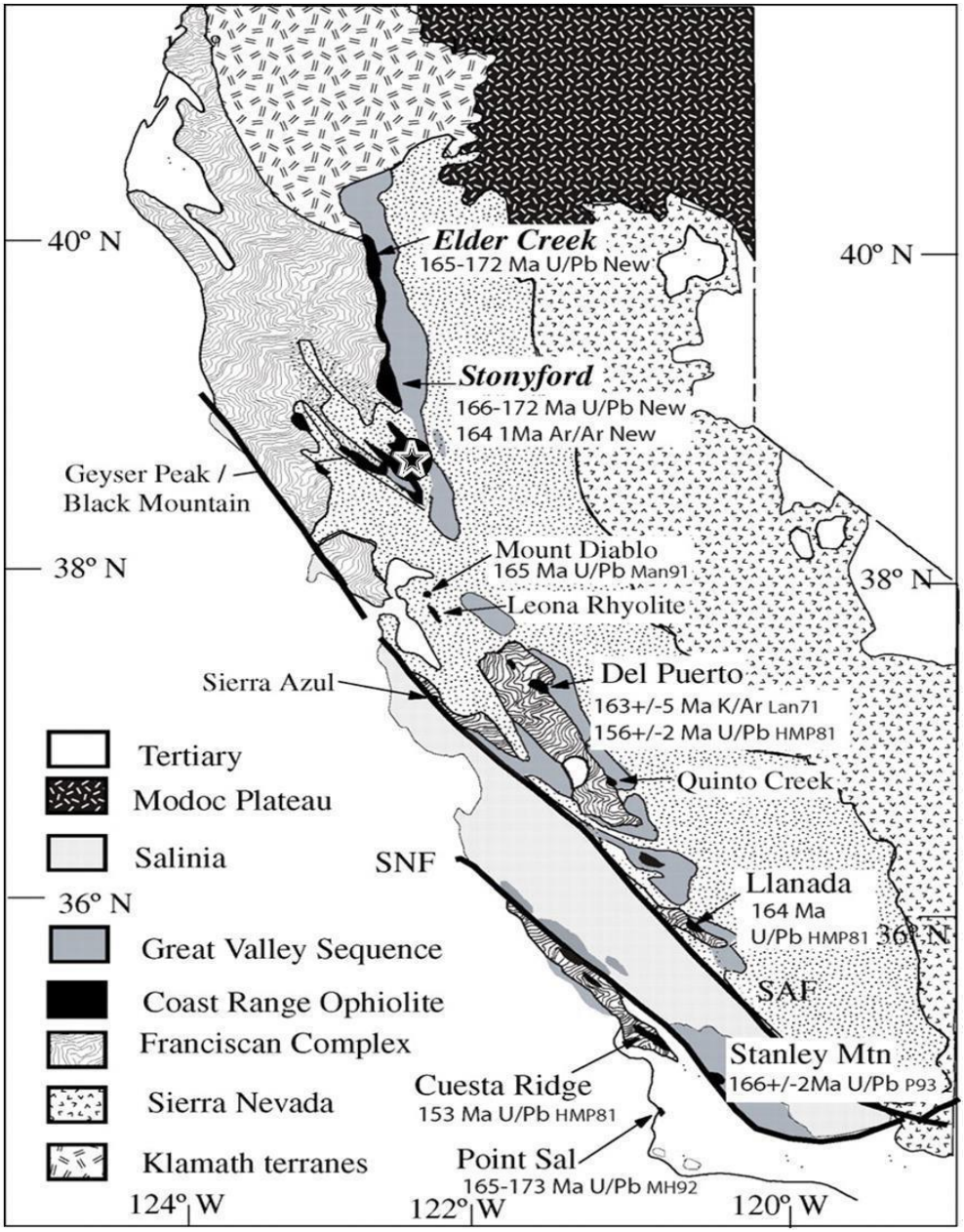

Figure 1. Geologic map of the Coast Range, with the ophiolite exposures in solid black, and the star indicating the location of McLaughlin Natural Reserve in Western California (modified from Choi et al., 2008).

Figure 2. Global distribution of ophiolites, except Spain, Japan (peridotite massifs) and Portugal (peridotite intrusion). Modified from Etiope, G. (2017).

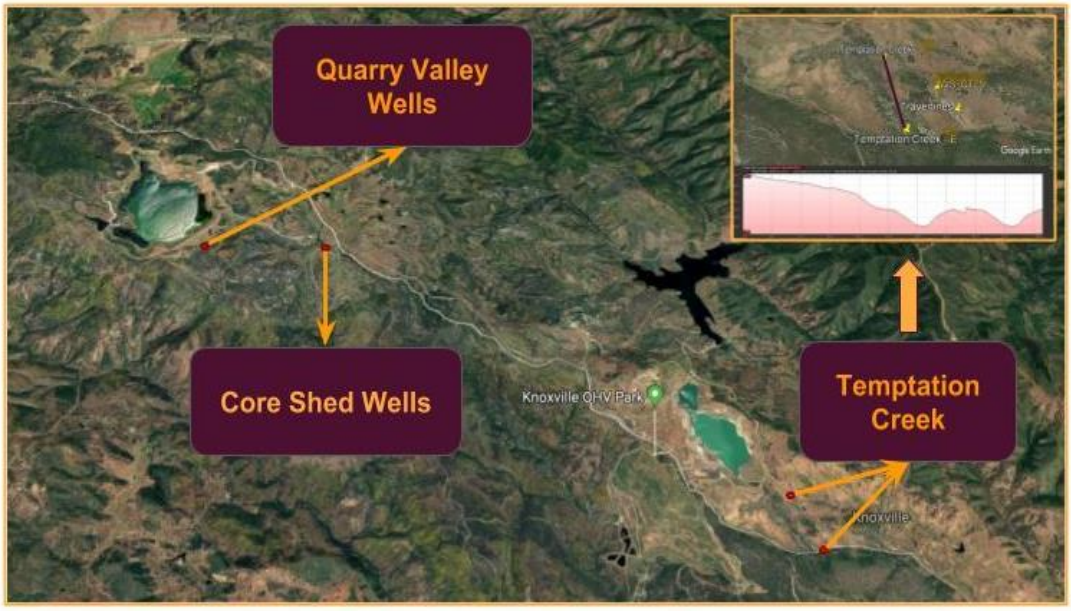

Figure 3. Aerial map of the three main sampling locations from McLaughlin Reserve created in Google Earth. The Quarry Valley Wells are named for historic quarrying of shale beds in the vicinity. The Core Shed Wells are named for the nearby regional core archive structure. A seasonally active groundwater-fed Temptation Creek is the third area for sample collection, with its two sampling points and their elevation profile shown inside the upper right box.

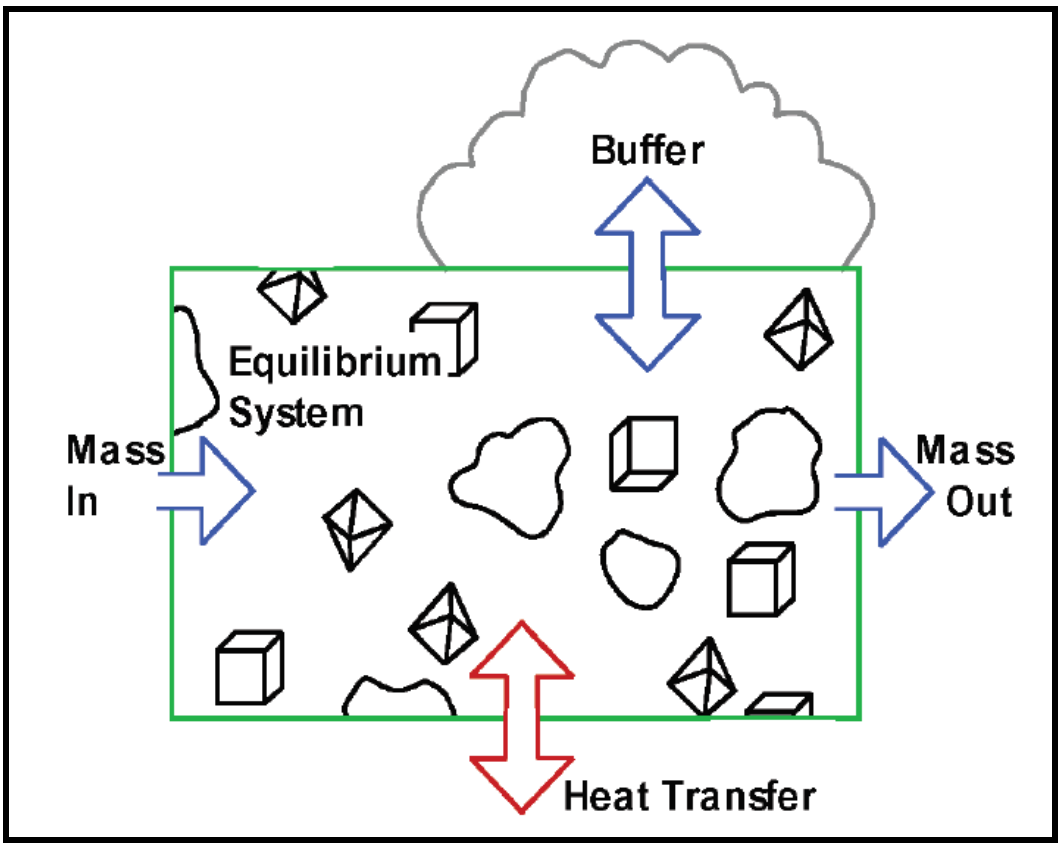

Figure 4. The conceptual model of the REACT mode simulation (Bethke & Yeakel, 2015).

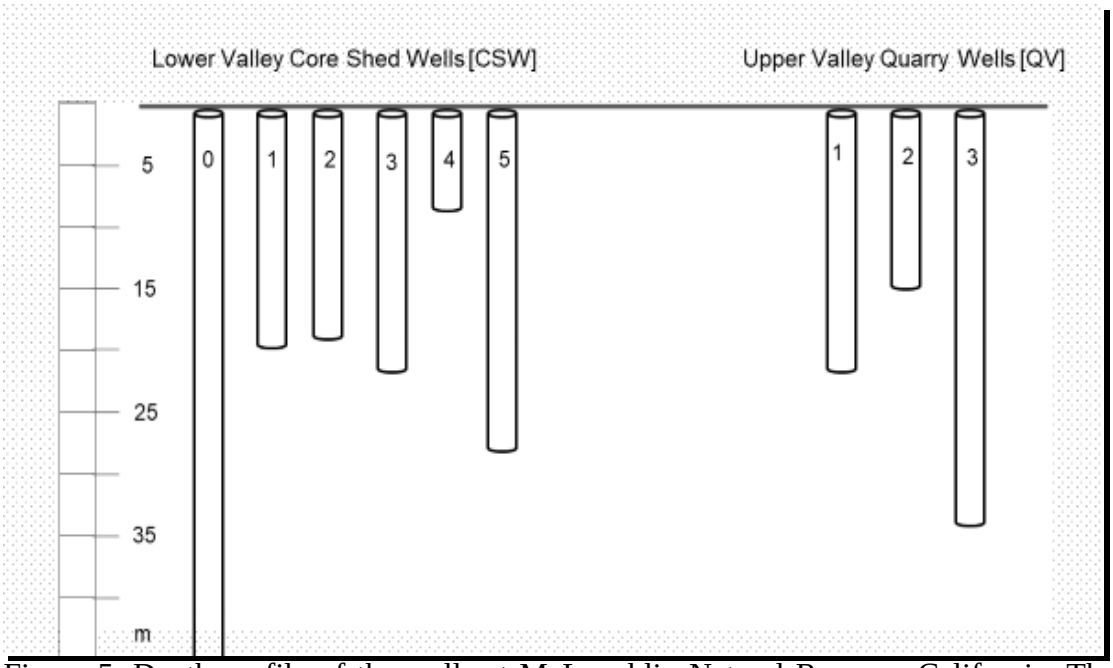

Figure 5. Depth profile of the wells at McLaughlin Natural Reserve, California. The QV wells are all within 3 m of the main QV1-1 well, from which rock cores were obtained. The CSW wells are within 5 m of the main CSW1-1 well, which also produced cores. The deepest well OCSW is 82 m deep.

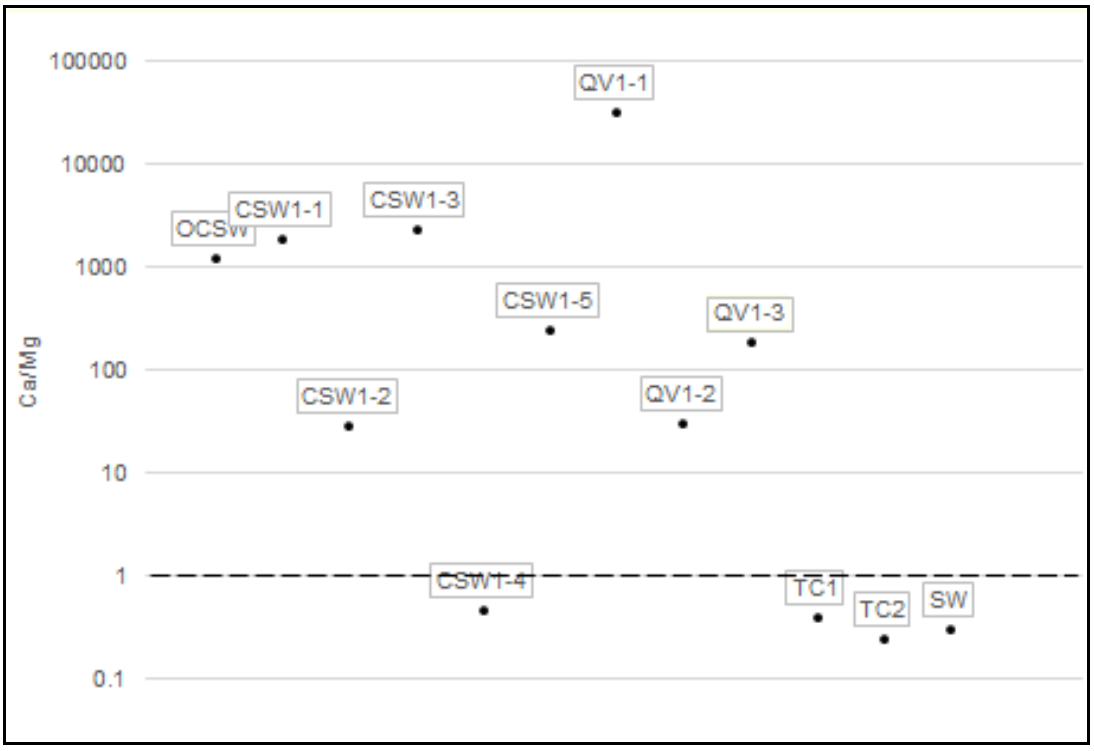

Figure 6. Calcium to magnesium ratios, plotted on Y-axis, with the sampling sites on X-axis. Ca/Mg ratios for TC1, TC2 and CSW1-4 are <1, being dominated by Mg^{+2}; while the rest of the wells (OCSW, CSW1-1, CSW1-2, CSW1-3, CSW1-5, QV1-1, QV1-2, QV1-3) are >1, dominated by Ca^{+2}.

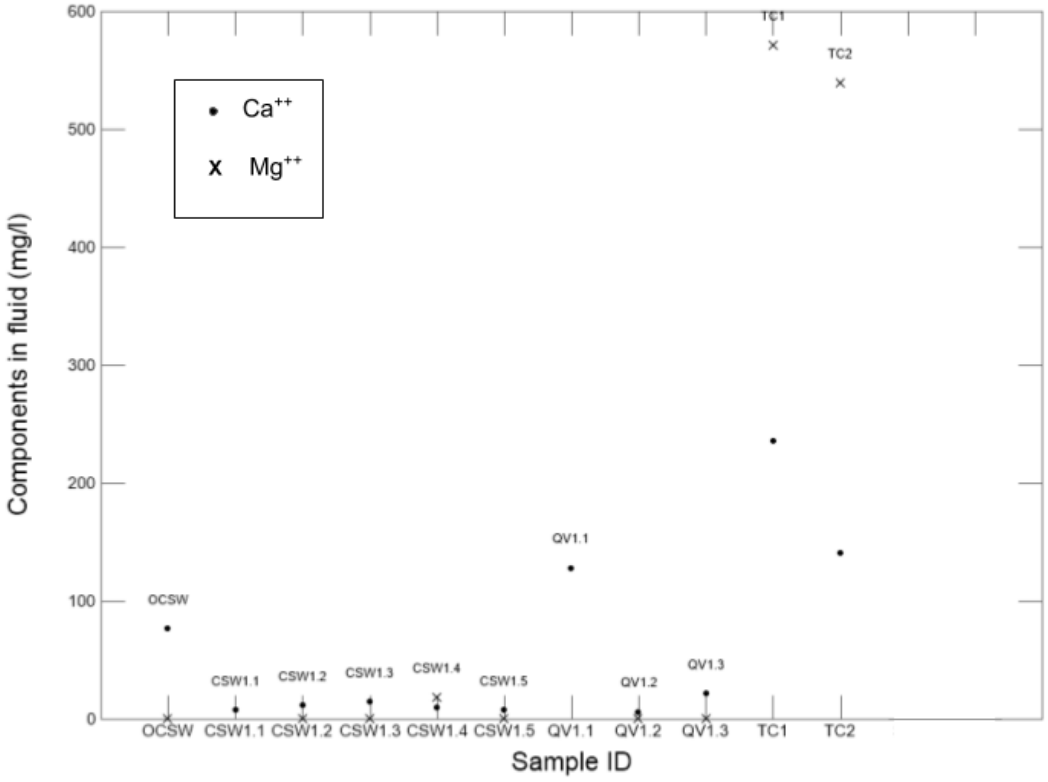

Figure 7. Ca^{+2} and Mg^{+2} ionic concentrations of CRO samples.

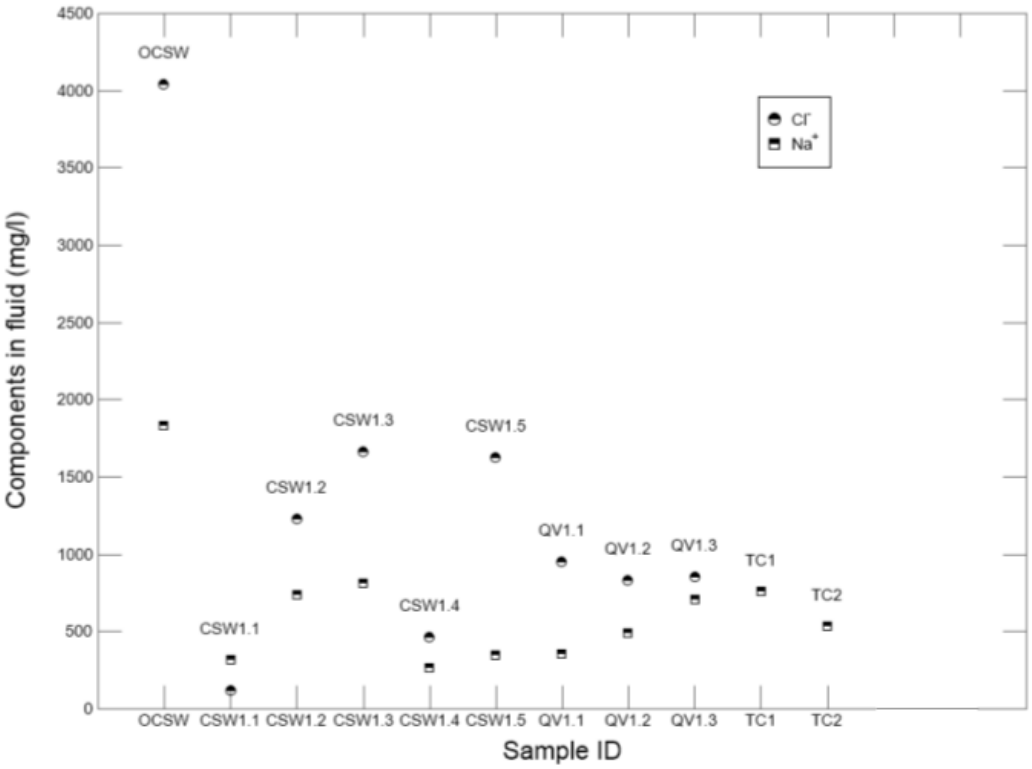

Figure 8. Sodium and Chloride ion composition present in the CRO samples.

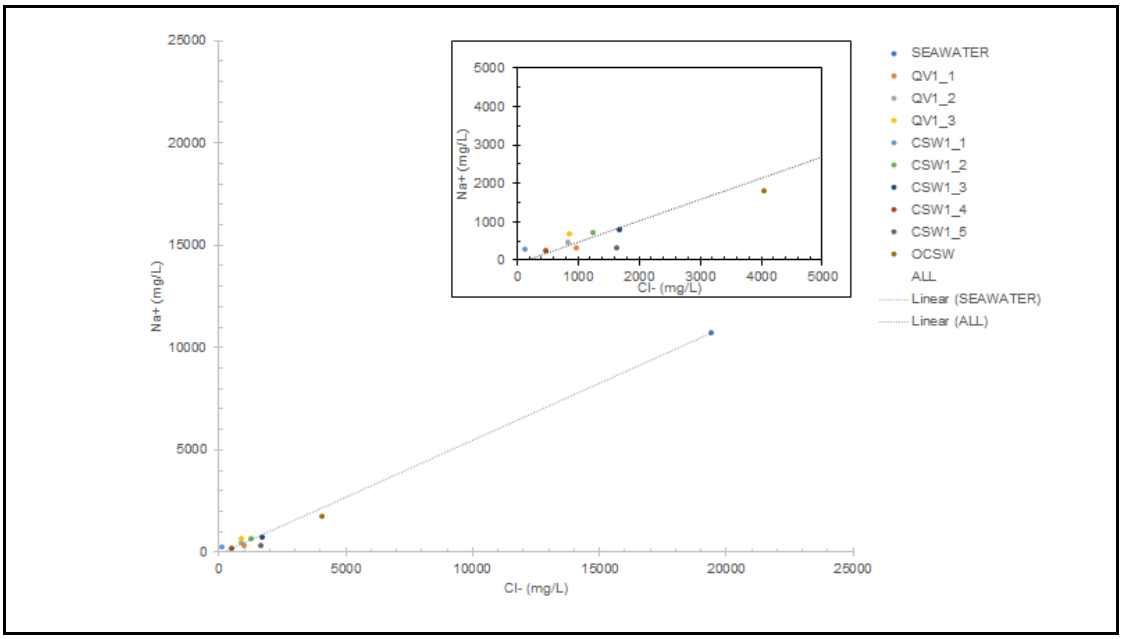

Figure 9. XY plot of sodium and chloride ion concentration with sodium ions plot on Y-axis, and chloride ions, on the X-axis. The trend-line passing through the seawater. Upper right box: Enlarged view of the samples shown along SW trendline.

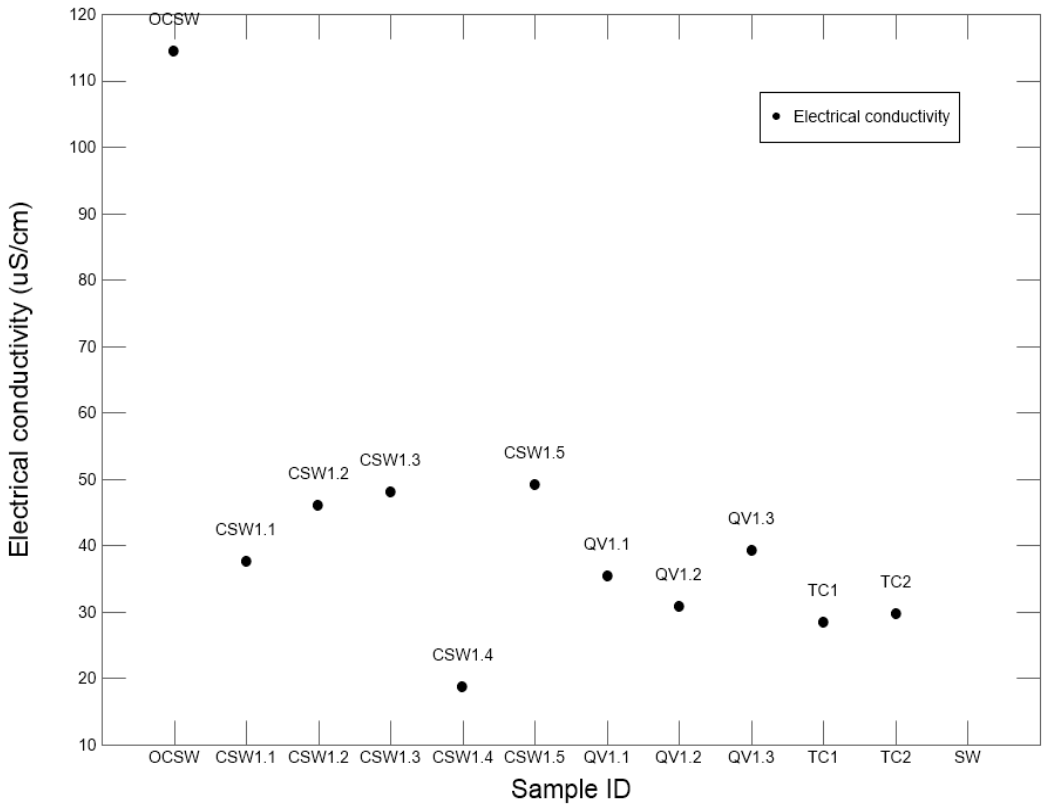

Figure 10. The electrical conductivity measured in mS/cm (milli second) and expressed here in uS/cm (micro second) for graphing the CRO samples.

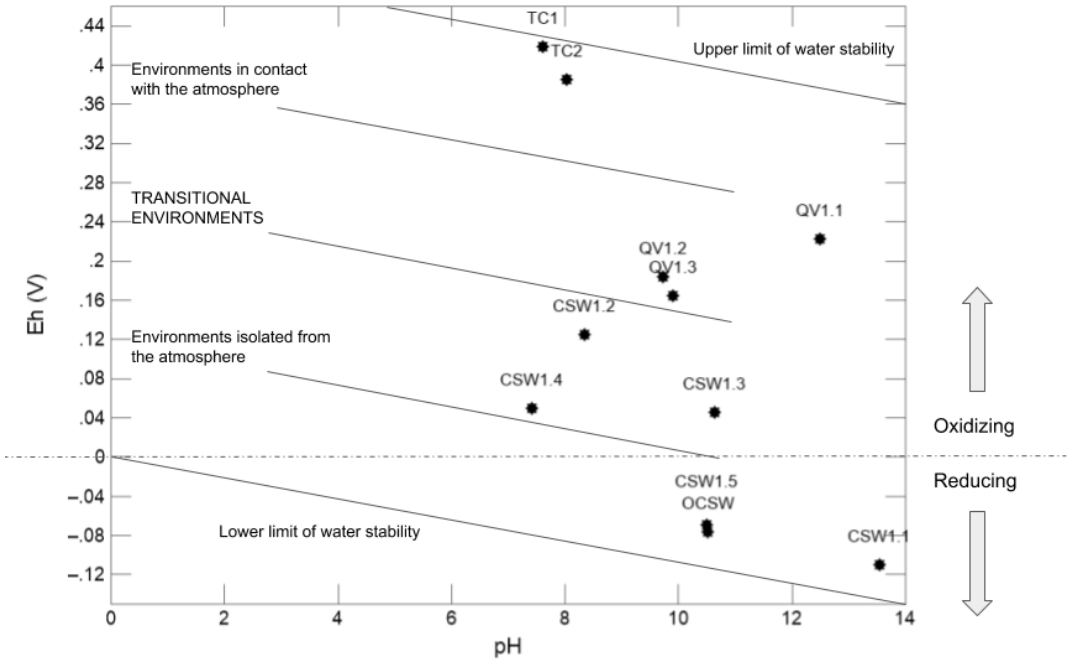

Figure 11. Based on the classic Eh-pH ranges for natural environments (Garrels and Christ,1965), OCSW, CSW1-1, and CSW1-5 show strongly reducing values (environment isolated from atmosphere), whereas TC1 and TC2 show oxidizing values for environments in contact with the atmosphere.

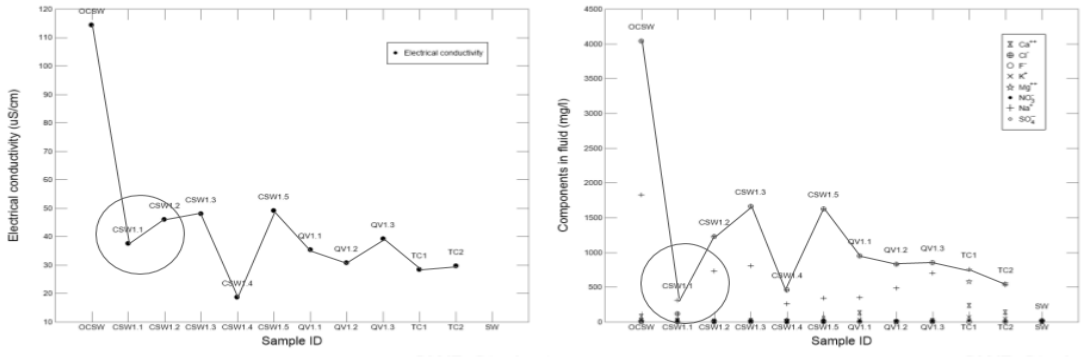

Figure 12. The graph profiles for the electrical conductivity (as a proxy for total dissolved solids) on the left, and the graph for the ionic concentrations of samples, on the right. Both graphs show similar graph profile curves, with the exception of CSW1-1.

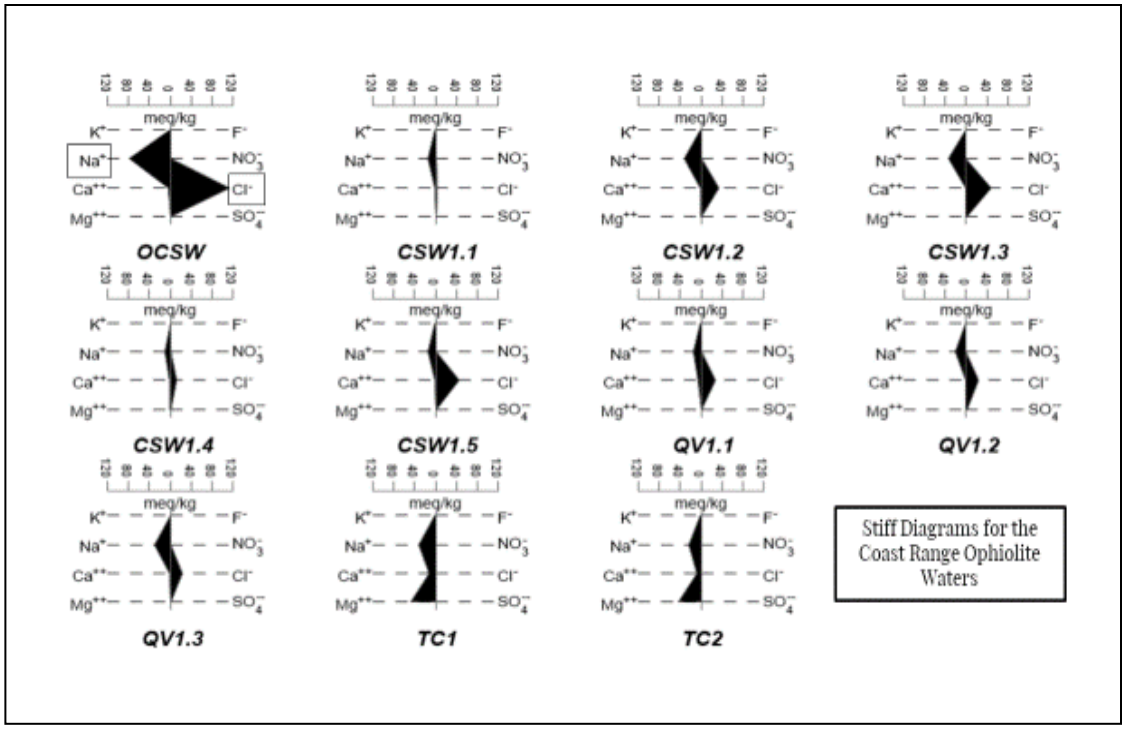

Figure 13. Stiff diagrams made in GWB showing the major ionic makeup and the compositional variations/similarities as a visual graphic for CRO samples.

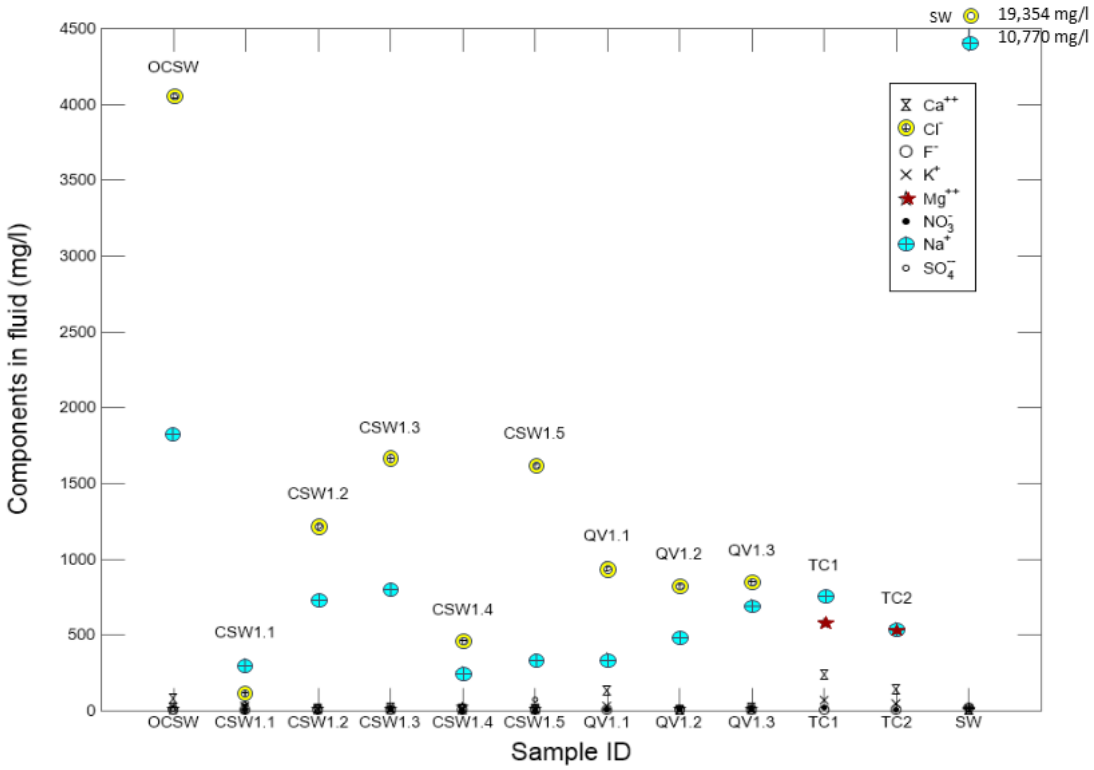

Figure 14. Ionic makeup of the 2017 CRO waters and. Overall, the ionic concentrations of all the CRO samples show that the Coast Range fluid samples distinguish themselves from other waters due to their high Na^{+}- Cl^{-} concentrations, followed by the high Mg^{+2} and Ca^{+2} concentrations.

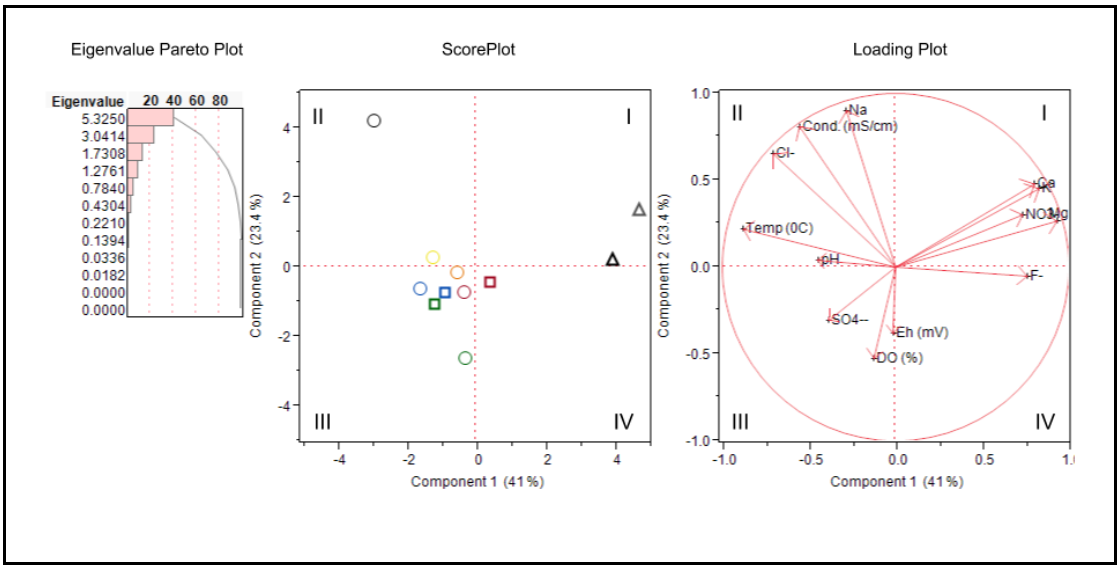

Figure 15: Principal components analysis results with Eigenvalue Pareto Plot (on the left), Score Plot (in the middle), and Loading Plot (on the right). In the Score Plot, the triangles (black and dark gray) represent Temptation Creek TC1 and TC2, circles (light gray, yellow, orange, pink, light blue, light green) as Core Shed Wells, and squares (red, dark blue, dark green) as Quarry Valley Wells.

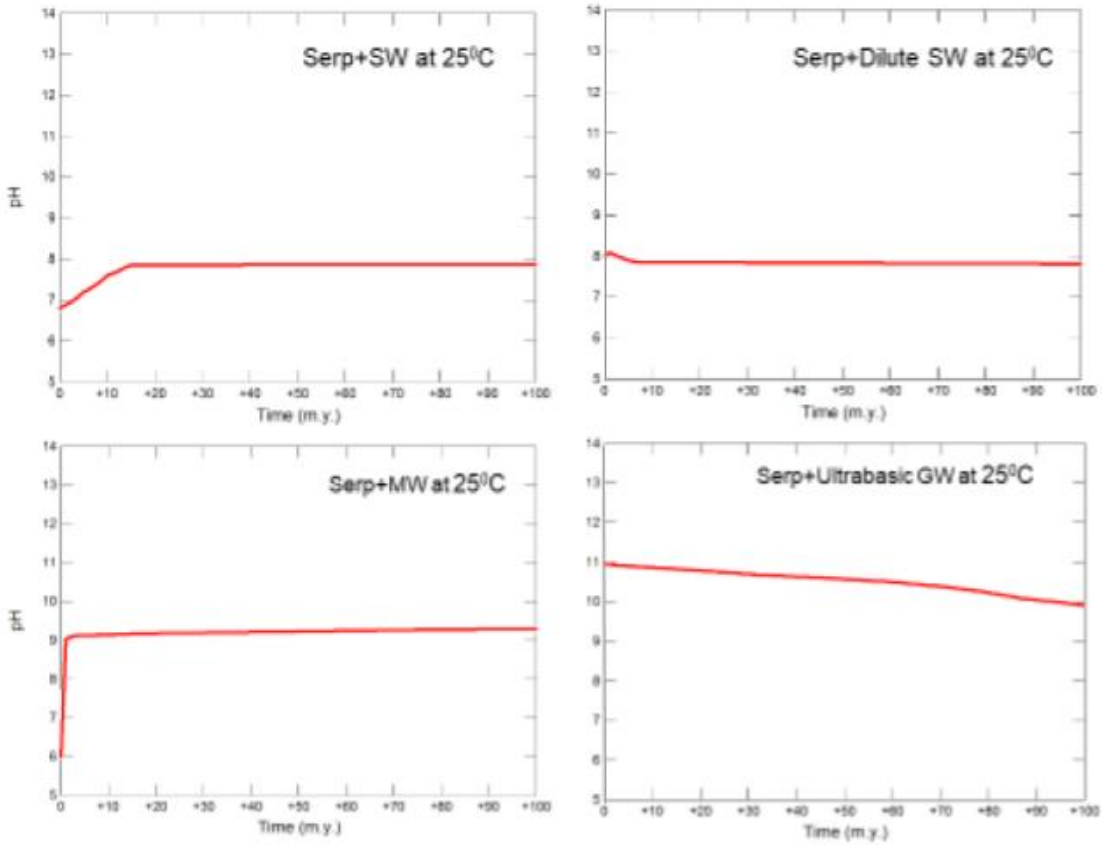

Figure 16: GWB REACT mode simulation for changing pH over the course of 100 million years at 25^0C.

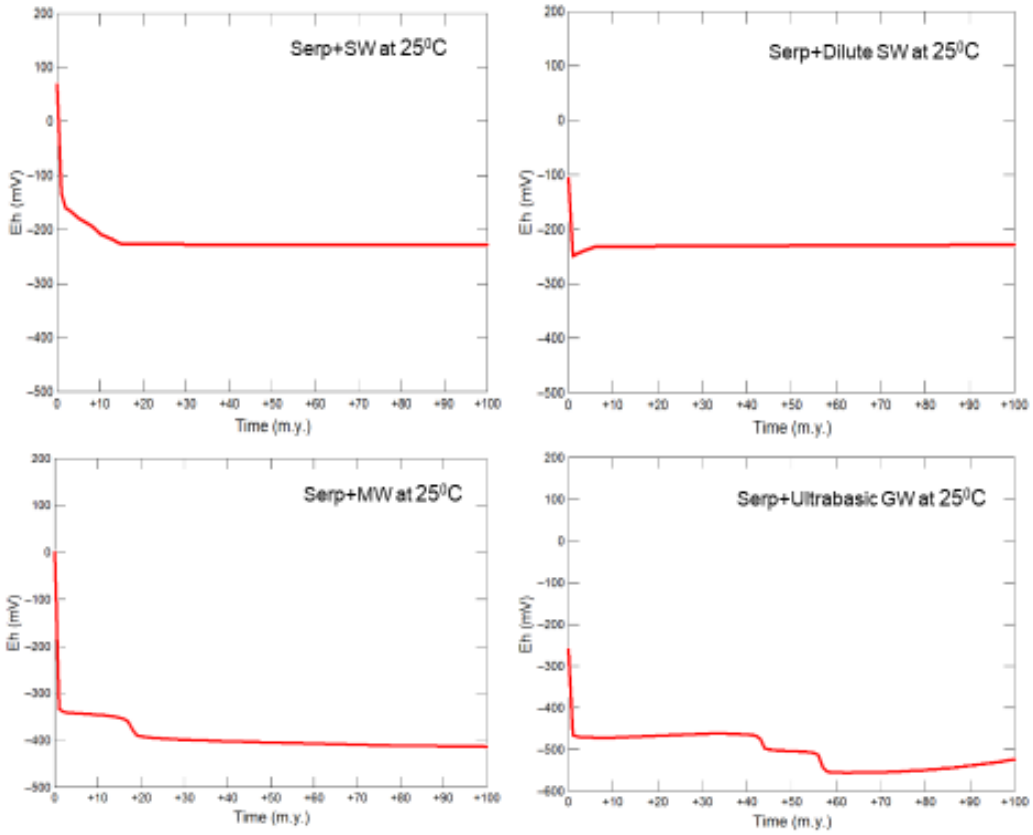

Figure 17: GWB REACT mode simulation for changing Eh (mV) over the course of 100 million years at 25^0C.

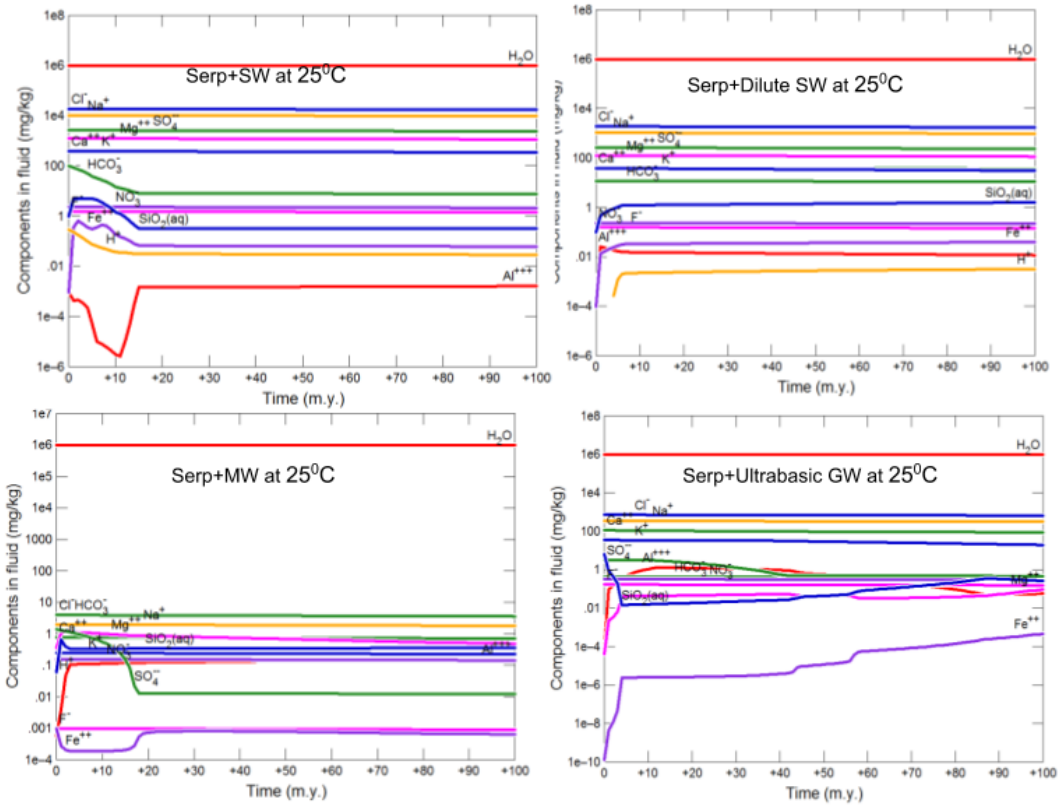

Figure 18: GWB REACT mode simulation for changing fluid composition (mg/kg) over the course of 100 million years at 25^{0}C.

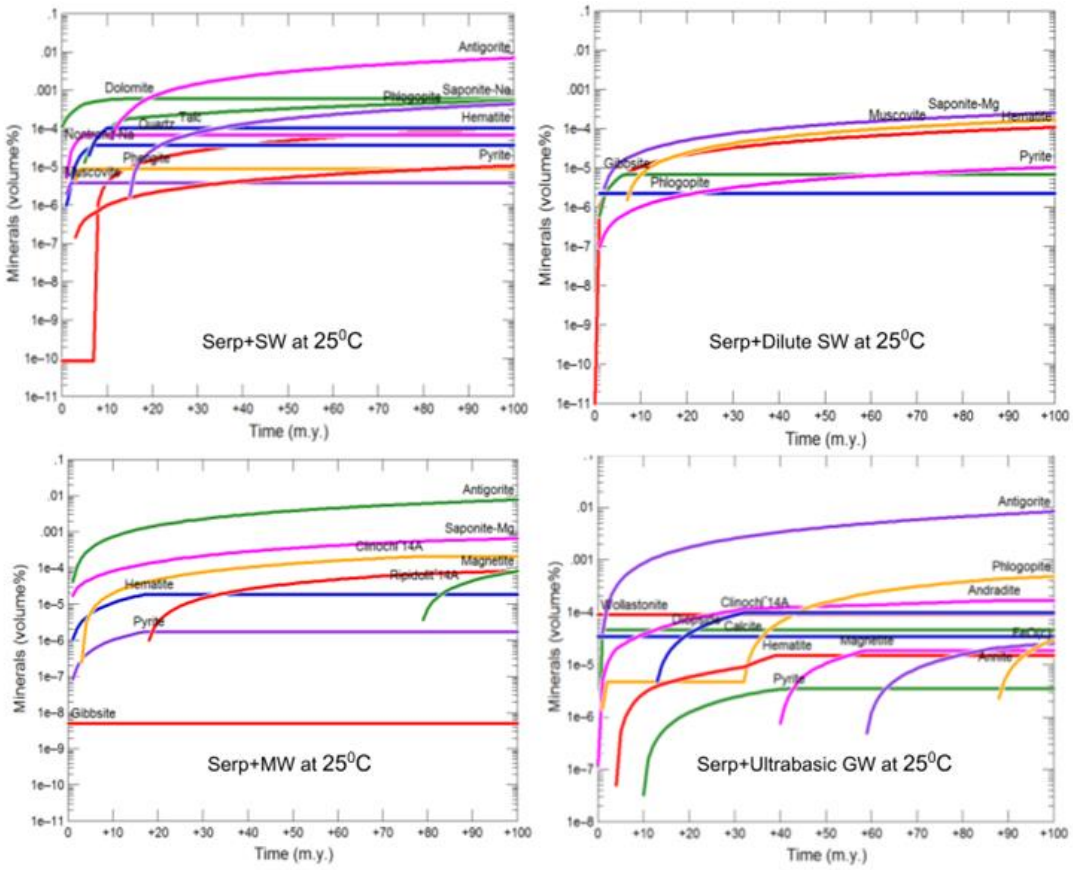

Figure 19: GWB REACT mode simulation for changing mineralogy (volume%) over the course of 100 million years at 25^0C.

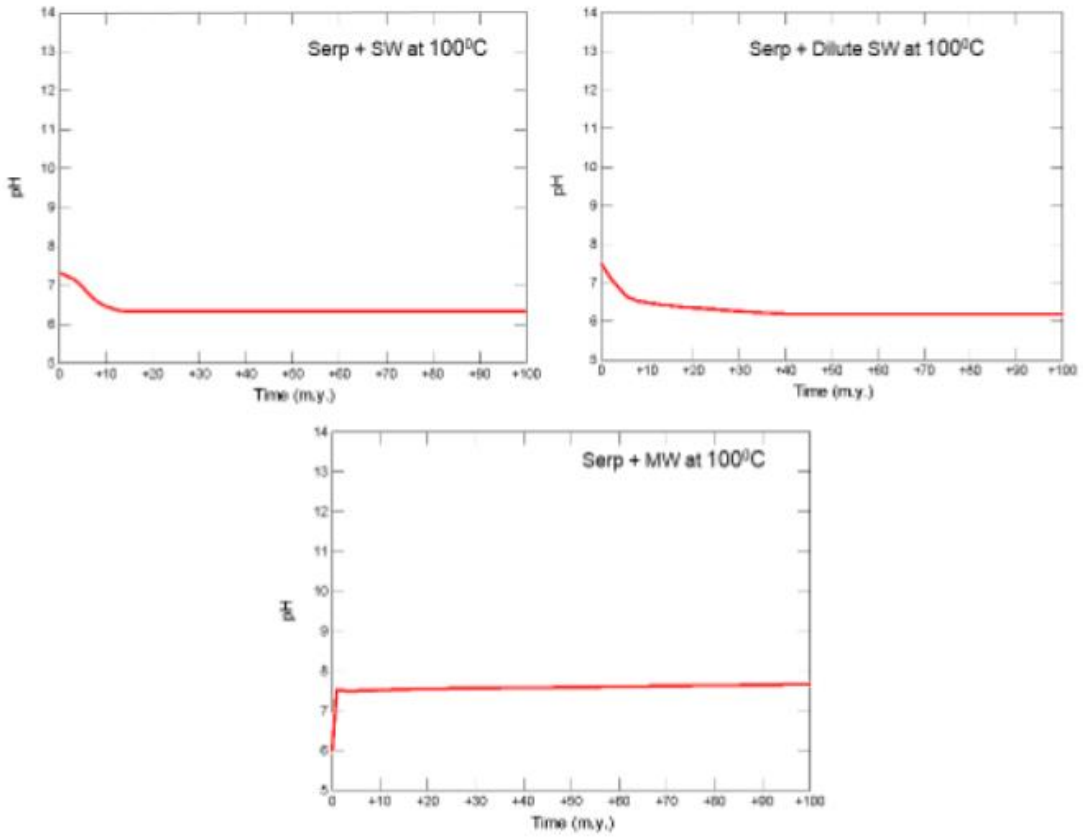

Figure 20: GWB REACT mode simulation for changing pH over the course of 100 million years at 100^0C.

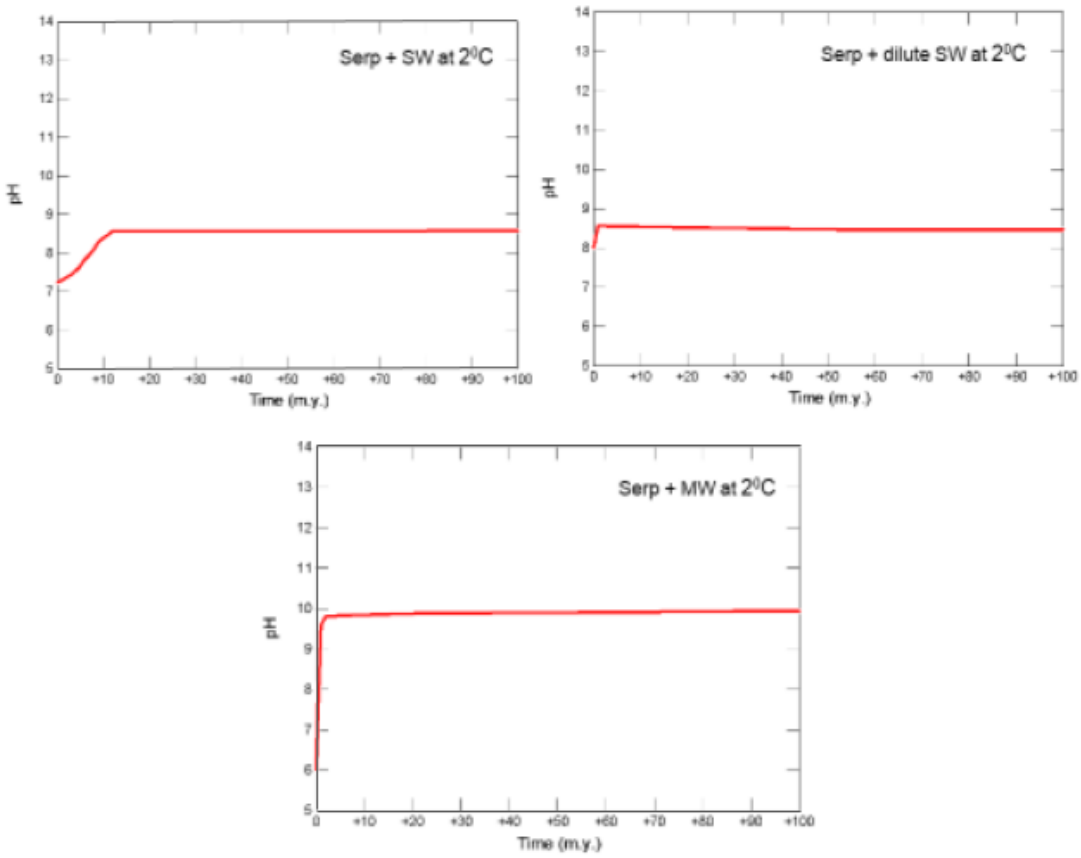

Figure 21: GWB REACT mode simulation for changing pH over the course of 100 million years at 2^0C.

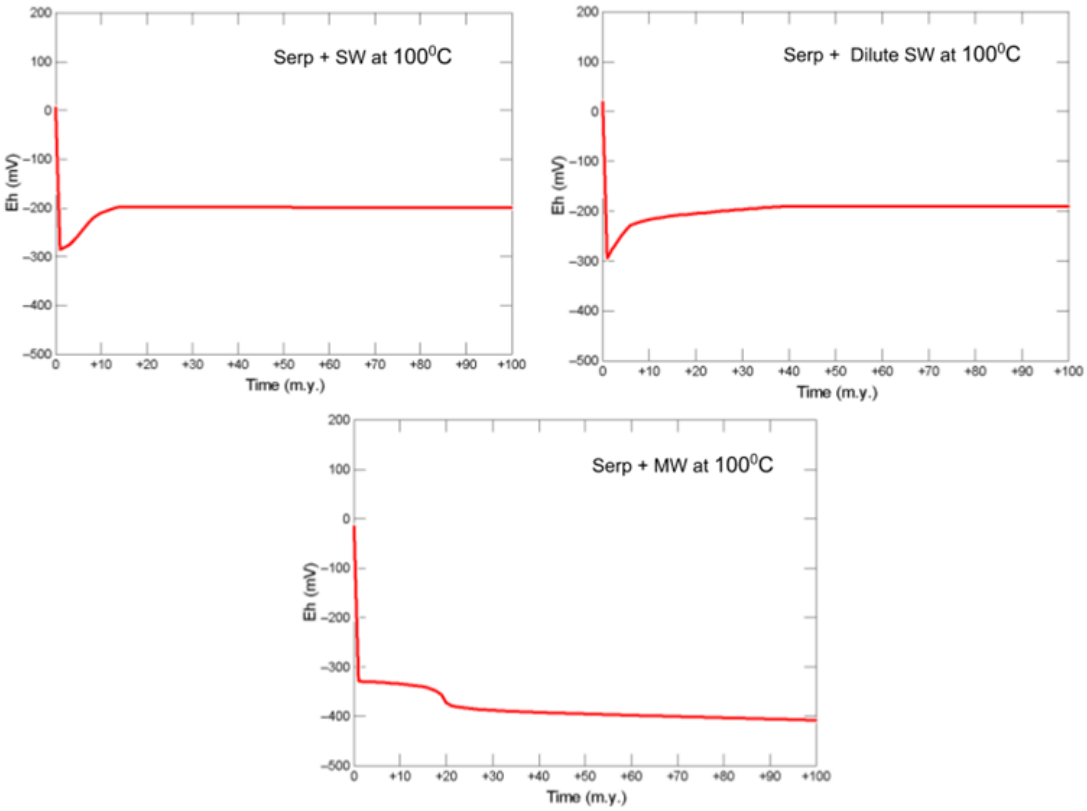

Figure 22: GWB REACT mode simulation for changing Eh (mV) over the course of 100 million years at 100^0C.

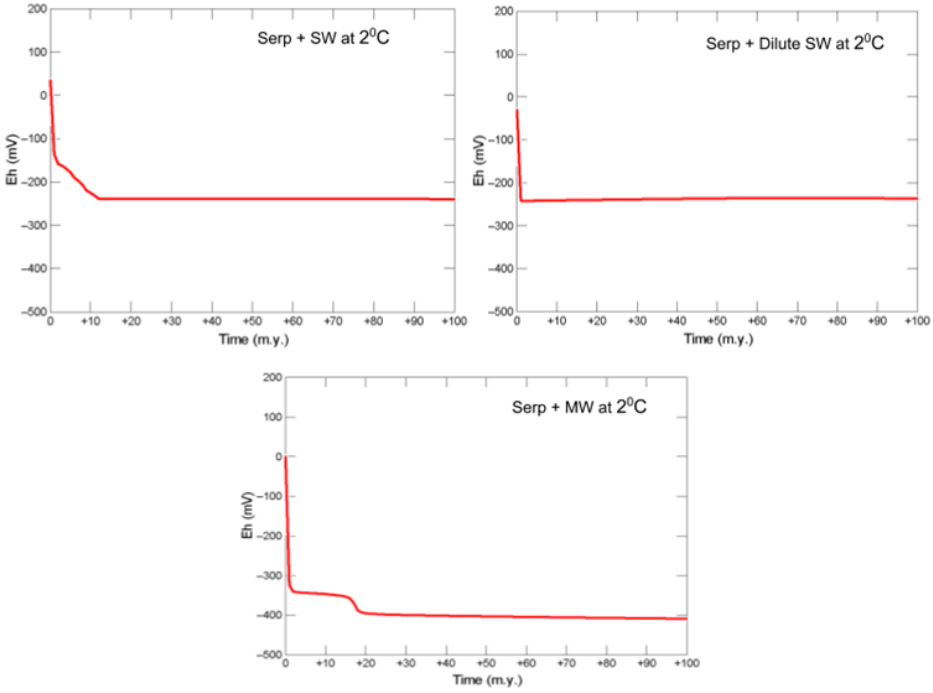

Figure 23: GWB REACT mode simulation for changing Eh (mV) over the course of 100 million years at 2^{0}C.

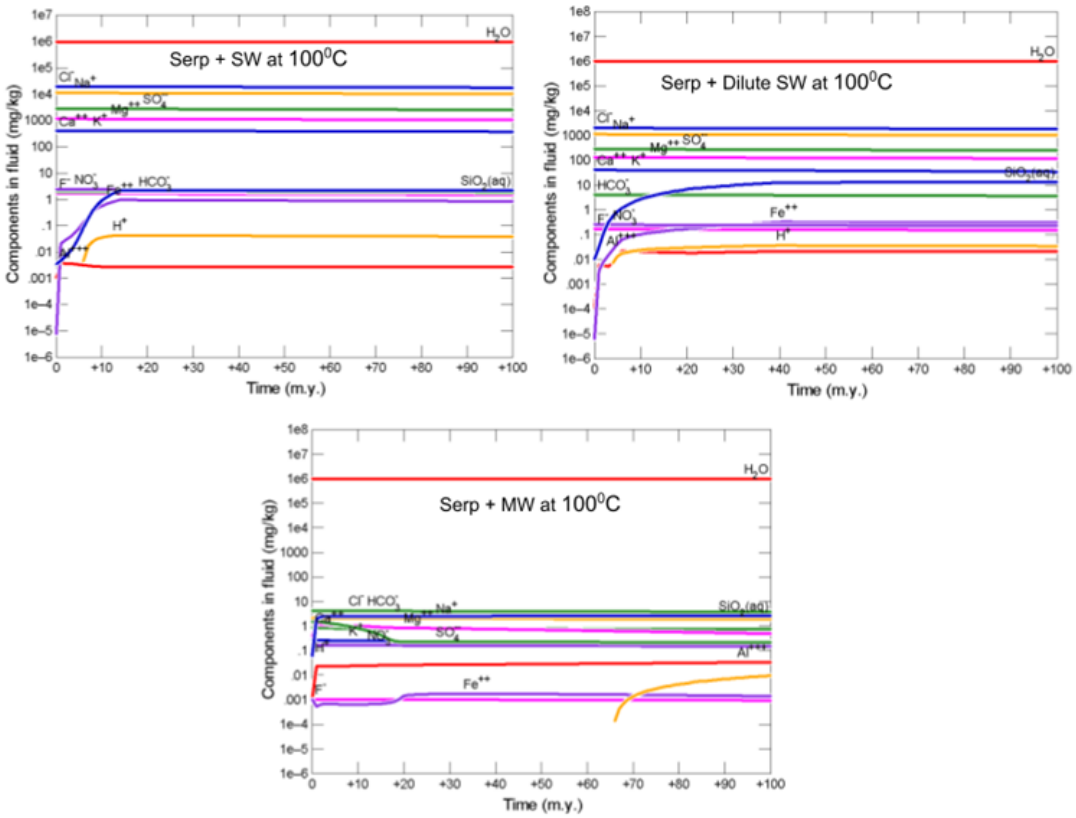

Figure 24: GWB REACT mode simulation for changing fluid chemistries (mg/kg) over the course of 100 million years at 100^{0}C.

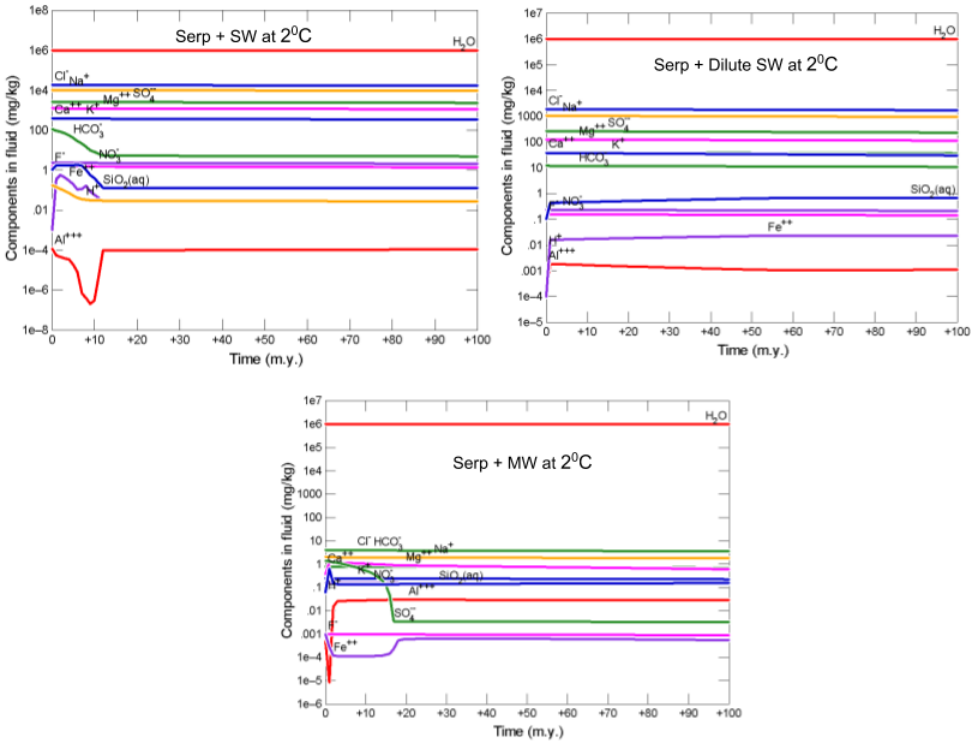

Figure 25: GWB REACT mode simulation for changing fluid chemistries (mg/kg) over the course of 100 million years at 2^0C.

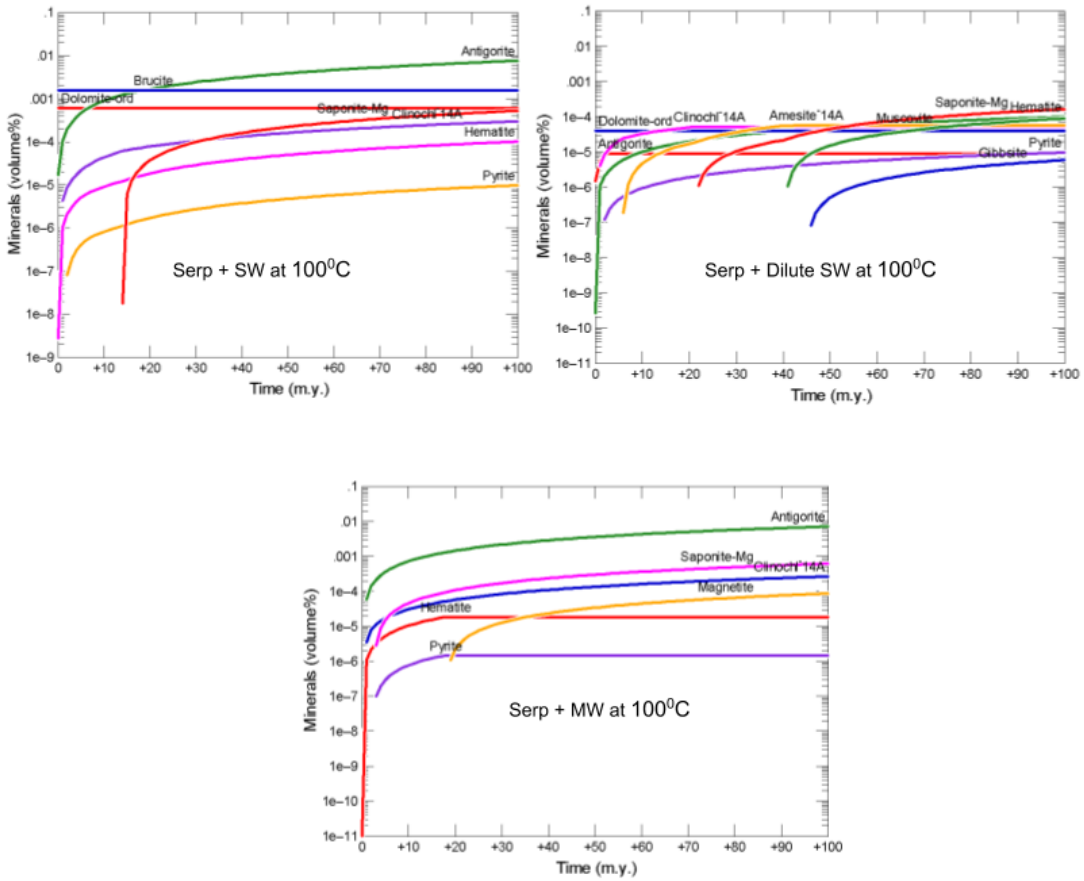

Figure 26: GWB REACT mode simulation for changing mineralogy (volume%) over the course of 100 million years at 100^{0}C.

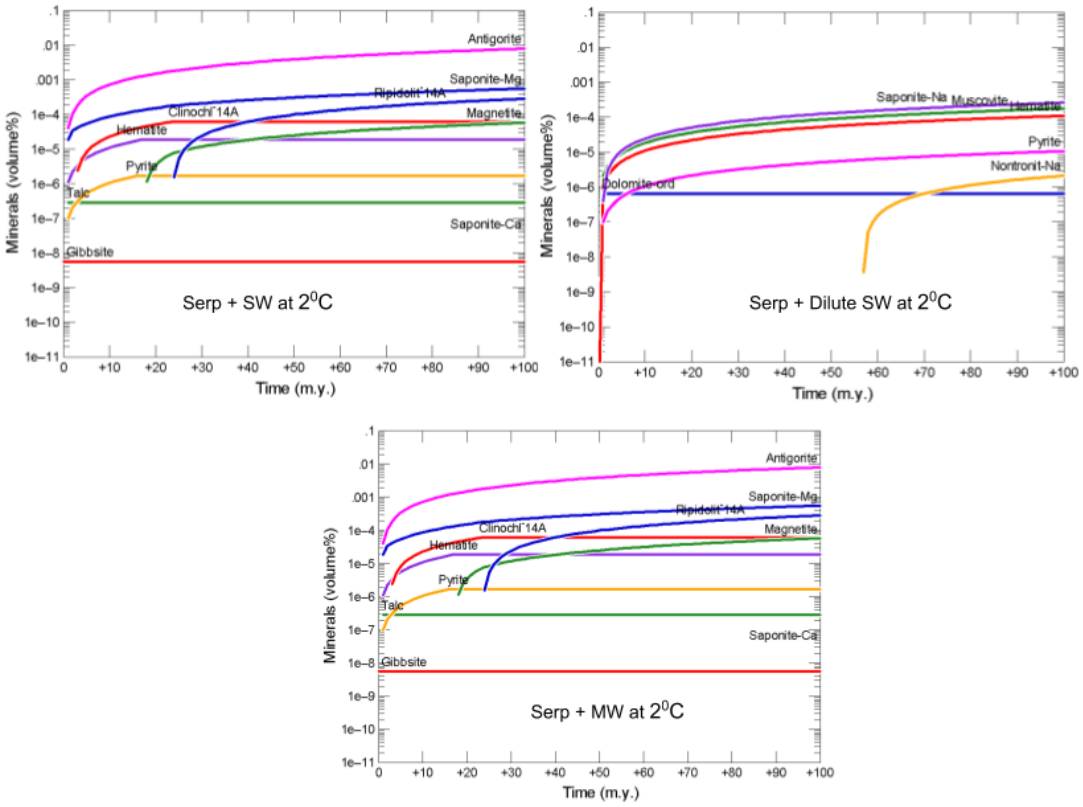

Figure 27: GWB REACT mode simulation for changing mineralogy (volume%) over the course of 100 million years at 2^0C.

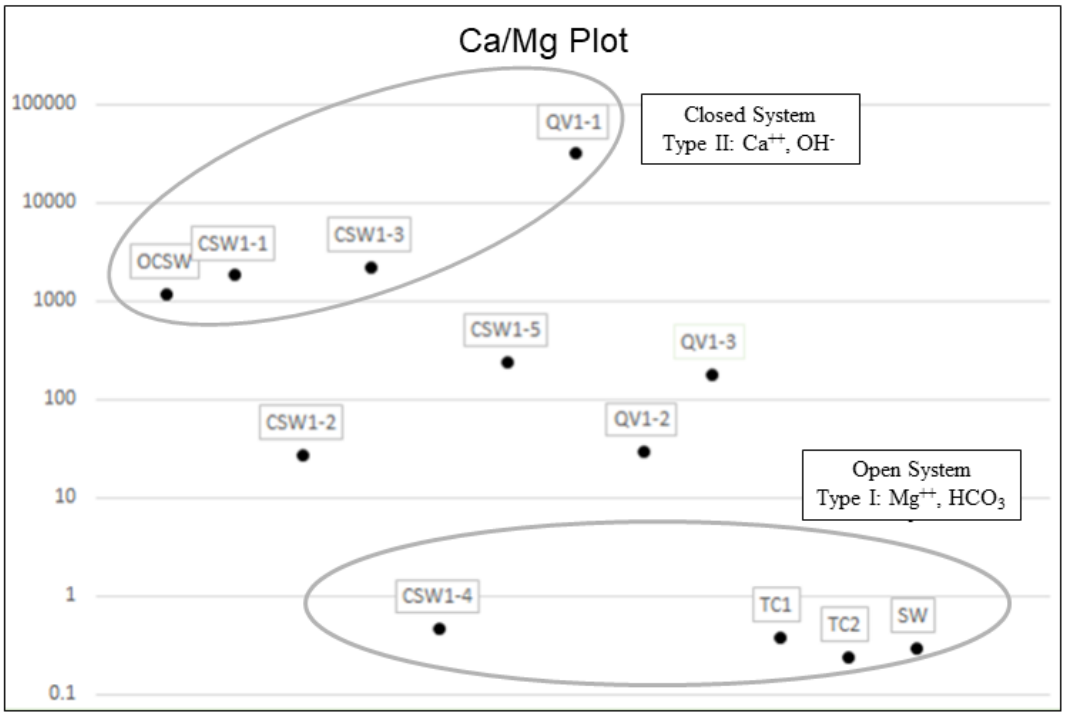

Figure 28: Type I, Type II and the mixed waters, based upon the Ca/Mg ratios. TC1, TC2 and CSW1-4 are Type I, open system waters. OCSW, CSW1-1, CSW1-5, and QV1-1 are the Type II, closed system waters. CSW1-2, CSW1-5, QV1-2, and QV1-3 are the mixed waters.

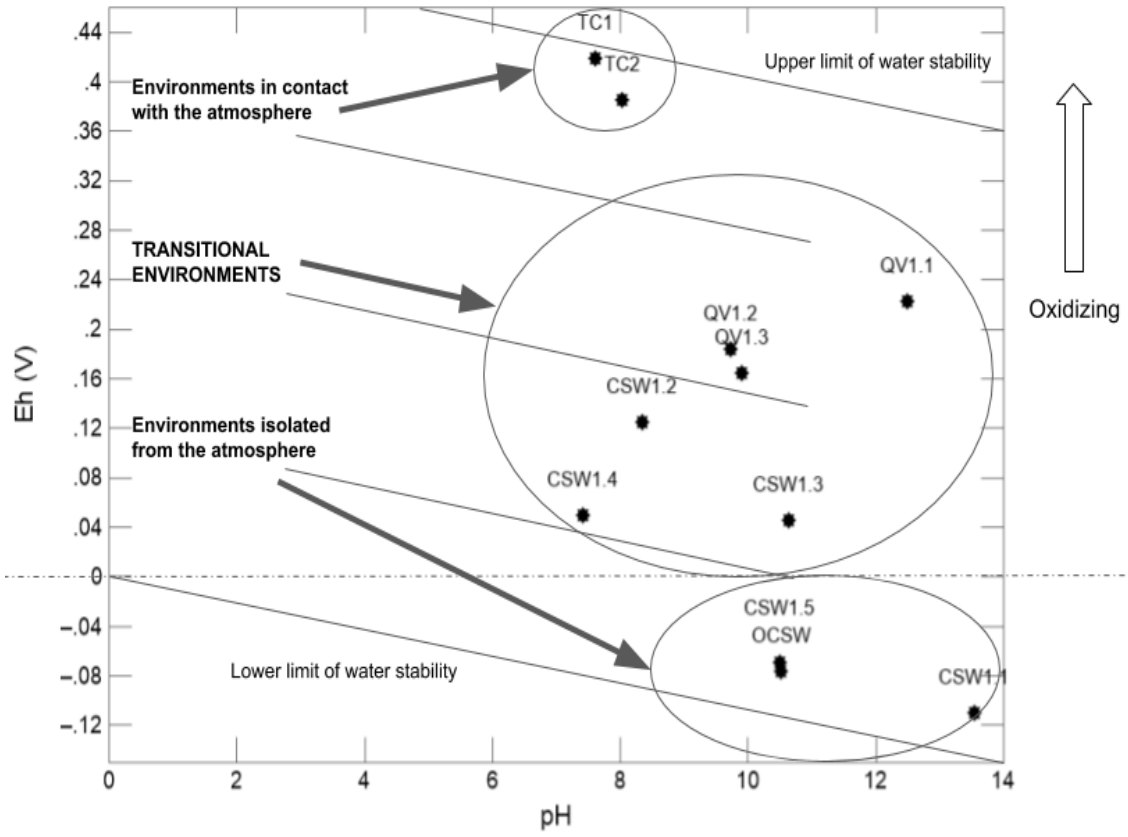

Figure 29. Eh-pH plot (modified from Garrels and Christ plot for limits of the natural environments, show OCSW, CSW1-1, and CSW1-5 as being strongly reducing. The wells CSW1-4, CSW1-3, CSW1-2, QV1-3, and QV1-2 show decreasing reducing trend with QV1-1 as the least reducing well. TC1 and TC2 are oxidizing waters.

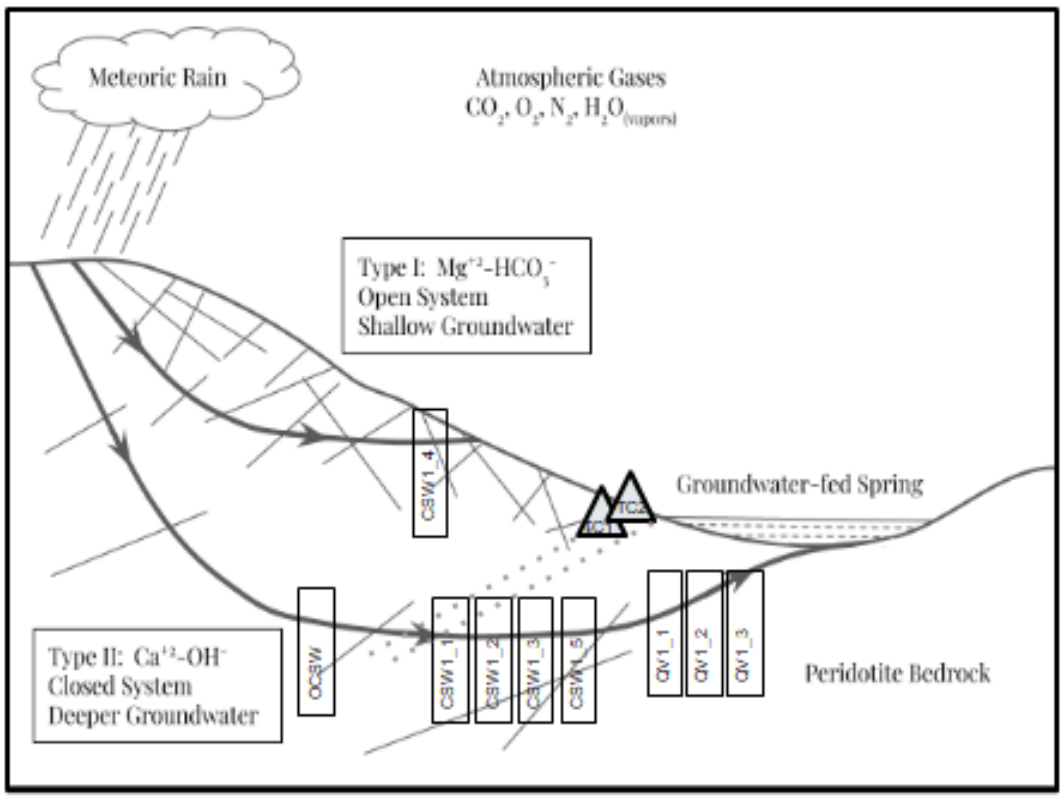

Figure 30. Summary of bedrock-water interactions taking place at the Coast Range ophiolite, as a framework for grouping CRO waters.

Table 1: The inputs used in GWB modeling. Geochemist's Workbench (GWB) REACT mode was used to model the low temperature alteration of a serpentinization-influenced water package passing through serpentinite rich environment. Three types of input waters were used: meteoric water, seawater, and a 10% seawater solution.

Parameters	Descriptions
Antigorite	0.5 mol/kg
Beidellite-Mg	0.1 mol/kg
Brucite	0.05 mol/kg
Clinochl-7A	0.1 mol/kg
Greenalite	0.2 mol/kg
Magnetite	0.05 mol/kg
Total mass input of solids	1 mol/Kg
Temperature	25^0C
Porosity	0.1
Water	1 kg free water + 0.1 kg/year
Initial pH	8
Time Frame	100 my
Pressure	1.0 bar
Type of water-rock system	Water dominated

Table 2: Ionic composition of regional precipitation (MW) at Menlo Park, California, from 1957-1959 (from Berner & Berner, 1987).

Ionic composition of regional precipitation at Menlo Park, California (1957-1959)	
Ion	Concentration (in mg/l)
Na^{+}	2.0
K^{+}	0.25
Mg^{++}	0.37
Ca^{++}	0.79
Cl^{-}	3.43
$SO4^{--}$	1.39
NO3-	0.16
$NH4^{+}$	–
Ca-/Na^{+}	1.7
pH	6.0

Table 3: Ionic composition of seawater (SW) (from Berner & Berner, 1987).

Major Dissolved Components of Seawater for a Salinity of 35% (*P=1 atm, T=25^0 C)	
Ion	Concentration in g/Kg
Na^+	10.77
K^+	0.399
Mg^{++}	1.290
Cl^-	19.354
$SO4^{--}$	2.712
Ca^{++}	0.412
HCO_3^{-*}	0.12

Table 4: Field data collected in 2017. The environmental parameters noted on site were the pH, temperature (°C), conductivity (EC, in mS/cm), dissolved oxygen (DO, in mg/L), and oxidation reduction potential (ORP, in mV, corrected to Eh by addition of 200 mV to the value observed in the field). TC1 and TC2 data here is from December of 2012.

2017 Sample ID	Temp (°C)	Cond. (mS/cm)	DO (%)	ORP (Eh, mV)	pH	Depth (m)
OCSW	17.81	11.44	1.9	-76.6	10.52	82
CSW1-1	15.89	3.758	1.1	-110	13.54	19.5
CSW1-2	15.85	4.602	0.9	124.8	8.35	19.2
CSW1-3	15.69	4.794	0.7	45.2	10.64	23.2
CSW1-4	15.34	1.86	19.5	49.6	7.42	8.8
CSW1-5	15.89	4.905	0.9	-69.2	10.5	27.4
QV1-1	15.55	3.526	2	222.1	12.49	23
QV1-2	17.35	3.073	3.6	183.7	9.73	14.9
QV1-3	15.93	3.918	4.8	163.9	9.9	34.6
TC1	14.24	2.833	1.32		7.61	
TC2	13.3	2.963			8.03	

Table 5. Ionic Composition of the CROMO samples from 2017 (expressed in mg/L)

	Ionic Composition of the CROMO samples from 2017 (expressed in mg/L)							
2017 Sample ID	F-	NO3-	SO4-2	Cl-	K+	Na+	Mg+2	Ca+2
OCSW	0.018		9.437	4041	24.33	1822	0.06	76.13
CSW1-1	0.22	0.262	40.444	113.62	31.28	312.8	<0.0038	7.42
CSW1-2	0.164		3.791	1229	11.3	728.6	0.38	11.2
CSW1-3	0.012	0.272	10.061	1663	11.69	802.6	0.006	14.36
CSW1-4	0.082	0.413	25.783	462.6	5.21	256.5	17.9	8.91
CSW1-5	0.058	0.388	70.488	1625	6.71	336.8	0.027	6.9
QV1-1	0.17	0.321	3.252	950	34.51	347.1	<0.0038	127.6
QV1-2	0.07	0.623	7.375	831	4.84	480.9	0.18	5.66
QV1-3	0.042	0.773	8.084	854	7.16	701.8	0.109	21.02
TC1	0.185	18.023			67.34	753.9	571.3	235.7
TC2	0.482	1.889			47.81	531.2	539.3	140.3

Table 6: Principal components analysis data table. Bold blues values show significant, strong, positive linear correlation. Faint blue values are weak but significant positive correlation, with grey values showing no correlation. Faint red values show weak, negative correlation and bold red values shows strong, negative correlation (inverse relationship).

Correlations

	Temp (0C)	Cond. (mS/cm)	DO (%)	Eh (mV)	pH	F-	NO3-	SO4--	Cl-	K	Na	Mg	Ca
Temp (0C)	1.0000	0.6164	0.0269	0.0755	0.4080	-0.7526	-0.4559	0.1616	0.7115	-0.6037	0.4448	-0.7740	-0.5579
Cond. (mS/cm)	0.6164	1.0000	-0.3170	-0.3745	0.2581	-0.3801	-0.2367	0.0193	0.9404	-0.0949	0.8887	-0.2893	-0.0702
DO (%)	0.0269	-0.3170	1.0000	0.1433	-0.3809	-0.2535	-0.1272	0.0953	-0.1532	-0.3746	-0.2681	-0.2150	-0.2691
Eh (mV)	0.0755	-0.3745	0.1433	1.0000	-0.0995	-0.1308	-0.1378	-0.5367	-0.1933	-0.2628	-0.2433	-0.2132	-0.0414
pH	0.4080	0.2581	-0.3809	-0.0995	1.0000	-0.1791	-0.4158	0.3357	0.2027	-0.0992	-0.0575	-0.5330	-0.2731
F-	-0.7526	-0.3801	-0.2535	-0.1308	-0.1791	1.0000	0.1888	-0.2389	-0.5804	0.6376	-0.3002	0.7034	0.4885
NO3-	-0.4559	-0.2367	-0.1272	-0.1378	-0.4158	0.1888	1.0000	-0.2691	-0.3570	0.7462	0.0565	0.7538	0.7871
SO4--	0.1616	0.0193	0.0953	-0.5367	0.3357	-0.2389	-0.2691	1.0000	0.0622	-0.3661	-0.3534	-0.3682	-0.4851
Cl-	0.7115	0.9404	-0.1532	-0.1933	0.2027	-0.5804	-0.3570	0.0622	1.0000	-0.3324	0.8058	-0.4659	-0.2212
K	-0.6037	-0.0949	-0.3746	-0.2628	-0.0992	0.6376	0.7462	-0.3661	-0.3324	1.0000	0.0962	0.8369	0.9248
Na	0.4448	0.8887	-0.2681	-0.2433	-0.0575	-0.3002	0.0565	-0.3534	0.8058	0.0962	1.0000	-0.0040	0.1719
Mg	-0.7740	-0.2893	-0.2150	-0.2132	-0.5330	0.7034	0.7538	-0.3682	-0.4659	0.8369	-0.0040	1.0000	0.8306
Ca	-0.5579	-0.0702	-0.2691	-0.0414	-0.2731	0.4885	0.7871	-0.4851	-0.2212	0.9248	0.1719	0.8306	1.0000

APPENDICES

Supplementary material that is pertinent to data accuracy and precision, and other technical details, are included in the following pages.

Table A-1: Making dilutions for IC calibrations using the Standard Stock Solutions. Start by using stock solutions, and making green coded, most concentrated calibration standards for cations, then for anions. Select the cation cal std 6, dilute this solution to make blue coded calibration standards. Select the anion cal std 7, dilute this solution to make orange coded calibration standards.

IONS [0.01 TO 5 mg/L)	Stock conc.	FINAL CONCENTRATIONS IN 50 ML VIAL							
		CAL STD 1	CAL STD 2	CAL STD 3	CAL STD 4	CAL STD 5	CAL STD 6	CAL STD 7	CAL STD8
UNITS	*mg/L*	*mg/L*	*mg/L*	*mg/L*	*mg/L*	*mg/L*	*mg/L*	*mg/L*	*mg/L*
Li	50	0.0005	0.0025	0.005	0.025	0.05	0.25	0.5	1
Na	200	0.002	0.01	0.02	0.1	0.2	1	2	4
NH4	400	0.004	0.02	0.04	0.2	0.4	2	4	8
K	200	0.002	0.01	0.02	0.1	0.2	1	2	4
Mg	200	0.002	0.01	0.02	0.1	0.2	1	2	4
Ca	1000	0.01	0.05	0.1	0.5	1	5	10	20
volume of stock solution needed (ml)	0.25	0.5	1						
volume of cal std 6 needed (ml)	0.1	0.5	1	5	10				
F	20	0.001	0.005	0.01	0.05	0.1	0.5	1	
Cl	100	0.005	0.025	0.05	0.25	0.5	2.5	5	
Nitrite	100	0.005	0.025	0.05	0.25	0.5	2.5	5	
Br	100	0.005	0.025	0.05	0.25	0.5	2.5	5	
nitrate	100	0.005	0.025	0.05	0.25	0.5	2.5	5	
PO4	200	0.01	0.05	0.1	0.5	1	5	10	
SO4	100	0.005	0.025	0.05	0.25	0.5	2.5	5	
volume of stock solution needed (ml)	0.125	0.25	1.25	2.5					
volume of cal std 7 needed (ml)	0.05	0.25	0.5						

Table A-2. Sample dilution protocol. Samples were titrated for chloride concentrations using HACH titration kit and diluted accordingly.

Sample	Target dilution	Sample Split Wt.	Water Wt.
OCSW	1_1000	0.0154	14.9738
CSW1-1	1_10	1.5088	13.7644
CSW1-2	1_1000	0.0156	14.9954
CSW1-3	1_1000	0.0152	14.9954
CSW1-4	1_100	0.1509	14.8188
CSW1-5	1_1000	0.015	15.0072
QV1-1	1_1000	0.0154	15.1095
QV1-2	1_1000	0.0154	15.0286
QV1-3	1_1000	0.0159	15.1456